Stony Brook University

Applications of Multichannel Brain Array Coils in Functional Neuroimaging

A Dissertation Presented

by

Sheeba Rani Arnold Anteraper

to

The Graduate School

in Partial Fulfillment of the

Requirements

for the Degree of

Doctor of Philosophy

in

Biomedical Engineering

Stony Brook University

August 2013

Stony Brook University

The Graduate School

Sheeba Rani Arnold Anteraper

We, the dissertation committee for the above candidate for the

Doctor of Philosophy degree, hereby recommend

acceptance of this dissertation.

Dr. Lilianne Mujica-Parodi – Dissertation Advisor
Associate Professor, Biomedical Engineering, Stony Brook University

Dr. Terry Button – Chairperson of Defense
Professor, Biomedical Engineering, Stony Brook University

Dr. Paul Vaska – Inside Member
Professor, Biomedical Engineering, Stony Brook University

Dr. Elisabeth Caparelli – Outside Member
Research Associate Professor, Social, Cognitive and Affective Neuroscience Center, Stony Brook University

This dissertation is accepted by the Graduate School

Charles Taber
Interim Dean of the Graduate School

Abstract of the Dissertation

Applications of Multichannel Brain Array Coils in Functional Neuroimaging

by

Sheeba Rani Arnold Anteraper

Doctor of Philosophy

in

Biomedical Engineering

Stony Brook University

2013

Deciphering signal from noise is a pre-requisite for making any scientific observation. Regardless of the imaging modality, any successful attempt in improving the Signal-to-Noise Ratio (SNR) brings about a wave of applications. The use of multichannel array coils in functional and structural magnetic resonance imaging (MRI) provides increased SNR, higher sensitivity, and parallel imaging capabilities. However, their benefits remain to be systematically explored in the context of resting-state functional connectivity MRI (fcMRI). In this work, signal detectability within and between commercially available multichannel brain coils, a 32-Channel (32Ch), and a 12-Channel (12Ch) were compared at 3 Tesla, in a high-resolution regime (2 mm-isotropic) to accurately map resting-state networks. The findings demonstrate that although the 12Ch coil can be used to reveal resting-state connectivity maps, the 32Ch coil provides increased detailed functional connectivity maps in a number of widely reported resting-state networks. The exploration of subcortical networks, which are scarcely reported due to limitations in spatial-resolution and coil sensitivity, also proved beneficial with the 32Ch coil. This was extended to the clinical realm by collecting resting-state fcMRI data from medication naïve patients with Social Anxiety Disorder and healthy control participants. Subcortical resting state networks from mid-brain and cerebellum seeds were compared between the two groups. Significant hyper-connectivity was observed in the patient group as compared to controls in all the subcortical networks that were explored. In addition, comparisons regarding the data acquisition time required to successfully map resting state networks indicated that scan time can be significantly reduced by 50% when a coil with increased number of channels (i.e., 32Ch) is used. Finally, the advantages of multichannel coils were explored with simultaneous multi-slice (SMS) acquisition scheme employing a range of repetition times (TR). Specifically, comparisons between 32Ch and 12Ch array coils revealed significant improvements in detecting functional connectivity maps at high temporal (TR=800 ms, SMS factor=7) and spatial resolutions. Switching to multichannel arrays in resting-state fcMRI could, therefore, provide both detailed functional connectivity maps and acquisition time reductions, which could further benefit imaging special subject populations, such as patients or pediatrics who have less tolerance in lengthy imaging sessions.

Table of Contents

List of Figures

List of Tables

List of Abbreviations

12Ch: 12 Channel

32Ch: 32 Channel

BOLD: Blood Oxygenation Level Dependent

aCompcor: anatomical Component based noise Correction method

CNR: Contrast-to-Noise Ratio

CSF: Cerebrospinal Fluid

DAN: Dorsal Attention Network

DMN: Default Mode Network

ECN: Executive Control Network

EPI: Echo Planar Imaging

fMRI: functional Magnetic Resonance Imaging

fcMRI: functional connectivity Magnetic Resonance Imaging

GM: Grey Matter

GRAPPA: Generalized Autocalibrating Partially Parallel Acquisition

HC: Healthy Controls

HCMN: Hippocampal Cortical Memory Network

LSAS: Liebowitz Social Anxiety Scale

RF: Radio Frequency

SAD: Social Anxiety Disorder

SN: Salience Network

SNR: Signal-to-Noise Ratio

tSNR: time-series Signal-to-Noise Ratio

WM: White Matter

Acknowledgments

Dr. Helmut Strey, the Graduate Program Director, for re-adopting me to the Department of Biomedical Engineering at Stony Brook University. Dr. Lilianne Mujica-Parodi, my dissertation advisor, for giving me the opportunity to work on one of the most exciting topics in the field today. The chairperson of my dissertation committee, Dr. Terry Button and the rest of the members Dr. Paul Vaska, and Dr. Elisabeth Caparelli for their time and willingness to take part in the mentoring process. Mrs. Anne Marie Dusatko for all the timely help. All my previous teachers, especially, Dr. Thomas Ernst, Dr. Linda Chang and Dr. James Goldfarb for introducing me to the wonderful world of Magnetic Resonance Imaging. Professor John Gabrieli, Director of the Athinoula A. Martinos Imaging Center at McGovern Institute for Brain Research, and my dear team, Dr. Atsushi Takahashi and Mr. Steven Shannon for their endless kindness. Dr. Susan Whitfield-Gabrieli from Massachusetts Institute of Technology, Dr. Larry Wald and Dr. Boris Keil from Athinoula A. Martinos Center for Biomedical Imaging at Massachusetts General Hospital, Dr. Alice Sawyer and Dr. Stefan Hofmann from Boston University, and Dr. Heather Urry from Tufts University deserve a special mention for their contributions at various stages of this dissertation. Such an endeavor would have been impossible without the constant support from my family and friends. Heartfelt thanks to all for making this happen. This dissertation is dedicated with utmost gratitude to Dr. Christina Triantafyllou, for her guidance over the last 7 years.

Vita, Publications and/or Fields of Study

Peer-Reviewed Publications

1. Ernst T, Chang L, Jovicich J, Ames N, **Arnold S**. Abnormal Brain Activation on Functional MRI in Cognitively Asymptomatic HIV Patients. Neurology Nov 12;59(9):1343-9, 2002.
2. Ernst T, Chang L, **Arnold S**. Increased Prefrontal Activation may be due to Up-regulated Oxidative Metabolism in HIV Brain Injury. Neuroimage Aug;19(4):1686-93, 2003.
3. Caparelli E, Tomasi D, **Arnold S**, Chang L, Ernst T. k-Space Based Motion Detection for Functional MRI, Neuroimage Oct;20(2):1411-8, 2003.
4. Chang L, Tomasi D, Yakupov R, Lozar C, **Arnold S,** Caparelli E, Ernst T. Neuroadaptation of the visual attention network in HIV-associated brain injury. Annals of Neurology Aug; 56:259-272, 2004.
5. Goldfarb J, **Arnold S**, Schapiro W, Reichek N. On the Cause of Spatial Displacement of Long T1 Species in Segmented Inversion Recovery Prepared Imaging. Magnetic Resonance in Medicine 54:481-485, 2005.
6. Goldfarb J, **Arnold S**, Roth M, Han J. T1 Weighted Magnetic Resonance Imaging Shows Fatty Deposition After Myocardial Infarction. Magnetic Resonance in Medicine 57:828-834, 2007.
7. Goldfarb J, **Arnold S**, Han J. Recent Myocardial Infarction: Assessment with Unenhanced T1 Weighted MR Imaging. Radiology 245:1, 245-250, 2007.
8. Goldfarb J, **Arnold S**, Roth M. Gadolinium pharmacokinetics of chronic myocardial infarcts: Implications for late gadolinium-enhanced infarct imaging. J Magn Reson Imaging 30:763-770, 2009.
9. Anteraper SA, Whitfield-Gabrieli S, Keil B, Shannon S, Gabrieli JD, Triantafyllou C. (2013): Exploring functional connectivity networks with multichannel brain array coils. Brain connectivity 3(3):302-15.
10. Goldfarb J and **Arnold Anteraper S**. Water-Fat Separation Imaging with Standard Magnetic Resonance bSSFP CINE Imaging of the Heart. Magnetic Resonance in Medicine (in press).
11. **Arnold Anteraper S**, Triantafyllou C, Sawyer A, Hofmann S, Gabrieli JD, Whitfield-Gabrieli S. Hyper-connectivity of Sub-cortical Resting State Networks in Social Anxiety Disorder. Brain Connectivity, (under review).

Selected Publications in Conference Proceedings

1. **Arnold S**, Ernst T, Tomasi D, Caparelli E, Chang L. Gender differences in brain activation during Visual Attention Processing. Proceedings of ISMRM, Toronto, Canada 2003.
2. **Arnold S**, Ernst T, Tomasi D, Caparelli E, Chang L. Gender differences in brain activation

during Visual Attention Processing. Proceedings of ISMRM, Toronto, Canada 2003.

3. **Arnold S**, Ernst T, Tomasi D, Caparelli E, Chang L. Residual Effects of Head Movement in fMRI. Proceedings of IEEE 29th Annual Northeast Bioengineering Conference, Newark, NJ, 2003.
4. **Arnold S**, Ernst T, Tomasi D, Caparelli E, Chang L. Effects of Hematocrit on BOLD fMRI during Visual Attention Processing. Proceedings of BMES Annual Fall Meeting, Tennessee, 2003.
5. **Arnold S**, Vogler M, Hinds O, Whitfield-Gabrieli S, Hamm M, Pfeuffer J, Triantafyllou C. Evaluation of EPI Geometric Distortion Correction using Phase Labeling for Additional Coordinate Encoding (PLACE). Proceedings of ISMRM, Hawaii, USA 2009.
6. **Arnold S**, Whitfield-Gabrieli S, Shannon S, Gabrieli G, Triantafyllou C. Improved BOLD Detection in the Working Memory Network using a 32 channel Phased Array Head Coil. Proceedings of ISMRM, Stockholm, Sweden 2010.
7. **Arnold S**, Whitfield-Gabrieli S, Shannon S, Gabrieli JD, Triantafyllou C, Reduction of Acquisition Time in Functional Connectivity MRI with 32-Channel Phased Array Head Coil, Human Brain Mapping, 17th Annual Meeting, Quebec City, Canada, 2011.
8. **Arnold S**, Whitfield-Gabrieli S, Shannon S, Gabrieli JD, Triantafyllou C, Improved Detection of Functional Connectivity MRI with 32-channel Phased Array Head Coil, International Society for Magnetic Resonance in Medicine, 20th Annual Meeting, Montreal, Canada, 2011.
9. **Arnold S**, Whitfield-Gabrieli S, Sawyer A, Gabrieli JD, Triantafyllou C, Altered Resting State Functional Connectivity in the Limbic System in Social Anxiety Disorder, Human Brain Mapping, 18th Annual Meeting, Beijing, China, 2012.
10. **Arnold S**, Triantafyllou C, Sawyer A, Hofmann S, Gabrieli JD, Whitfield-Gabrieli S, Altered Thalamostriatal Resting State Functional Connectivity in Social Anxiety Disorder, Third Biennial Conference on Resting State Brain Connectivity, Magdeburg, Germany, 2012.
11. **Arnold S**, Whitfield-Gabrieli S, Sawyer A, Gabrieli JD, Triantafyllou C, Alterations in Cerebellar Functional Connectivity in Social Anxiety Disorder, International Society for Magnetic Resonance in Medicine, 22nd Annual Meeting, Utah, USA, 2013.
12. **Arnold S**, Whitfield-Gabrieli S, Sawyer A, Gabrieli JD, Triantafyllou C, Macroscopic Effects of Susceptibility Gradients on Functional Connectivity MRI, Human Brain Mapping, 19th Annual Meeting, Seattle, USA, 2013.

Chapter 1

General Introduction

Functional MRI (fMRI) currently dominates the landscape of functional neuroimaging in terms of the number of publications per year. Although Blood Oxygen Level Dependent (BOLD) fMRI is instrumental in studying brain activity, and has made an impact particularly in the realm of cognitive neuroscience, precise localization of BOLD contrast is still a challenge, primarily because of imaging limitations such as low spatial resolution and partial volume effects. Efforts have been made to move to higher resolutions, but this is typically done at the cost of scan time (decreasing temporal resolution) so that adequate Signal-to-Noise Ratio (SNR) can be maintained. This augments the problem, because practice/habituation effects get introduced with additional scan time and degrades the image quality by making it prone to subject motion and fatigue effects. Furthermore, in a clinical setting, task-based fMRI might be difficult to execute because of poor subject compliance or cognitive deficits. Latest technological advances in high magnetic field strengths, multichannel array coils (to receive MR signal) and parallel imaging are promising tools to tackle these issues. The overall goal of the thesis is to use multichannel brain array coils for accurately identifying brain networks in the resting state in a short acquisition time. At the core of the thesis is the use of the 32-Channel (32Ch) coil to detect BOLD signal originating from task-free spontaneous low-frequency BOLD fluctuations (< 0.1 Hz). Correlation estimates of such intrinsic activity exhibit specific brain networks to provide functional connectivity MRI (fcMRI), which has gained acceptance as a viable research tool. Capability of the 32Ch coil in providing improved BOLD signal detection and potential scan time reduction

remains yet to be explored and evaluated systematically in the context of fcMRI. The objective of my dissertation research is to meet this goal and to explore potential clinical applications, particularly in the realm of neuropsychiatric disorders. Finally, the application of simultaneous multi-slice (SMS) acquisition in improving temporal resolution of fcMRI will be explored.

The improved sensitivity afforded by array coils was described in their first application (Roemer et al., 1990). Sensitivity increases (especially near the array) stems from the improved geometric coupling between small inductive elements and nearby spins compared to larger surface coils (Hayes and Axel, 1985). The array concept allows the sensitivity of the small surface coil to be extended over greater areas. The sensitivity benefit deep from the surface is smaller since the smaller diameter surface coils have steeper sensitivity drop-offs with depth (Hayes and Axel, 1985). But as the number of array elements (N_{ch}) that are used to tile a fixed area increases, the element size decreases. The added benefits of N_{ch} nearly independent measurements of the deep voxel therefore exactly cancel the effect of the increased drop-off. The net effect is sensitivity at the center of the brain that is comparable to the larger elements. Electro-magnetic simulation studies have been shown, that the best possible detection (ultimate SNR) in the center of a head-sized uniform spherical sample is already approachable with as few as 8 channels at 3T (Wiesinger et al., 2004). At the periphery, the sensitivity grows approximately linearly with the number of elements and therefore larger numbers of elements are required for approaching the theoretical SNR limit. Results from experimental coil array studies were found to be quantitatively in-line with the results obtained from simulation studies (Keil et al., 2012; Wiggins et al., 2009).

Although highly parallel arrays have been characterized extensively for their SNR advantages and parallel imaging capabilities (de Zwart et al., 2004; Triantafyllou et al., 2011;

Wiggins et al., 2006), only limited effort has been dedicated in monitoring their performance in the real-world scenario. The increased sensitivity from array coils in a time-series fMRI data set translates directly to higher BOLD contrast sensitivity. The BOLD contrast-to-noise ratio (CNR) is proportional to the time series signal-to-noise ratio (tSNR): CNR = - tSNR TE $\Delta R2^*$, where TE and $\Delta R2^*$ originates from tissue properties and is field dependent, but independent on other acquisition parameters. Interestingly, choices of head coil and voxel size affect BOLD CNR through tSNR. However, the interplay of these parameters for the detectability of resting state functional connectivity networks remains to be demonstrated.

The thesis is divided into three parts. The first part of the thesis (Chapter 2) provides a description of exploring functional connectivity networks with multichannel head coil in the high-resolution regime, without employing parallel imaging. The second part (Chapter 3) is a direct application of the work from Chapter 2 in the clinical domain. Finally, the last part of the thesis (Chapter 4) provides a summary of the protocol optimization work using SMS acquisitions (Feinberg et al., 2010; Setsompop et al., 2012) with 5 different SMS factors for the detection of resting-state fcMRI. In addition, Chapter 4 highlights the necessity of having multichannel arrays as a pre-requisite for providing a combination of high spatial and temporal resolution without trading off whole-head coverage. General conclusions are summarized in Chapter 5.

Chapter 2

Exploring Functional Connectivity Networks with Multichannel Brain Array Coils

Abstract

Using multichannel array head coils in functional and structural MRI provides increased Signal-to-Noise Ratio (SNR), higher sensitivity and parallel imaging capabilities. However, their benefits remain to be systematically explored in the context of resting state functional connectivity MRI (fcMRI). In this study, we compare signal detectability within and between commercially available multichannel brain coils, 32-Channel (32Ch) and a 12-Channel (12Ch) at 3T, in a high-resolution regime to accurately map resting state networks. We investigate whether the 32Ch coil can extract and map fcMRI more efficiently and robustly than the 12Ch coil using seed-based and graph-theory based analyses. Our findings demonstrate that although the 12Ch coil can be used to reveal resting state connectivity maps, the 32Ch coil provides increased detailed functional connectivity maps (using seed-based analysis) as well as increased global and local efficiency, and cost (using graph-theory analysis), in a number of widely reported resting state networks. Exploration of subcortical networks, that are scarcely reported due to limitations in spatial-resolution and coil sensitivity, also proved beneficial with 32Ch coil. Furthermore, comparisons regarding the data acquisition time required to successfully map these networks indicated that scan time can be significantly reduced by 50% when a coil with increased number

of channels (i.e. 32Ch) is used. Switching to multichannel arrays in resting state fcMRI could therefore provide both detailed functional connectivity maps and acquisition time reductions, which could further benefit imaging special subject populations, such as patients or pediatrics who have less tolerance in lengthy imaging sessions.

2.1 Introduction

Previous studies (Triantafyllou et al., 2011) have shown that in comparison to standard coils (single channel), multichannel arrays offer improvements in fMRI time-series SNR (tSNR) when medium to small size voxel volumes are used, whereas in larger voxel sizes the improvements are modest, primarily because physiological noise (originating from fluctuations such as cardiac, respiratory, and hemodynamic induced signal modulations) increases with voxel size. For example, 32Ch coil improves the tSNR of the $1.5\times1.5\times3$ mm^3 acquisition by 48% compared to 12Ch coil; the increase, however, is only 11% at low resolution ($5\times5\times3$ mm^3) (Triantafyllou et al., 2011). Additionally, higher resolution fMRI acquisitions could potentially increase spatial specificity and localization of the resting state networks, while minimizing partial volume effects and thru-plane signal dropouts, due to thinner slices.

Although the acquisition parameter space in fcMRI have already been investigated thoroughly by Van Dijk and colleagues (Van Dijk et al., 2010) the additive sensitivity from advances in multichannel array coils remains to be explored. In this study we therefore evaluate the detectability power of multichannel arrays in resting state fcMRI at a high resolution regime of Echo Planar Imaging (EPI), where we are expecting to achieve the biggest benefits from the high-N arrays. We investigate some of the most widely reported networks including the default mode network (DMN) (Greicius et al., 2003), the hippocampal-cortical memory network (HCMN) (Vincent et al., 2008), the dorsal attention network (DAN) (Corbetta and Shulman,

2002), the executive control network (ECN), and the salience network (SN) (Seeley et al., 2007). In order to investigate the SNR improvements in deeper brain regions with the 32Ch array we also examine seed-based connectivity in sub-cortical regions (basal ganglia network) of the brain. In addition, we evaluate the benefit of higher sensitivity of the 32Ch array coil by measuring the effective reduction in acquisition time to accurately map intrinsic correlations using fcMRI.

2.2 Methods

2.2.1 Data Acquisition

Data acquisition was performed on a Siemens 3T scanner, MAGNETOM Trio, a Tim System, (Siemens AG, Healthcare Sector, Erlangen, Germany), using two different commercially available Radio Frequency (RF) receive-only head coils; a 12Ch and a 32Ch brain array coils (Siemens AG, Healthcare Sector, Erlangen, Germany). The 32Ch array consists of 32 loop elements set in the soccer-ball geometry as described in the literature by Wiggins et al (Wiggins et al., 2006). The product version is a split-type design with the anterior part consisting of 12 elements and the posterior of 20 elements. The 12Ch coil is the vendor's "head matrix coil" product which is the default coil to the 3T Tim Trio system, Siemens. This coil combines 12 long elements in one ring. The whole-body transmit coil was used for excitation in both cases. The same 16 healthy volunteers (7 males), all right-handed, age range: 18-33 years, (mean age: 25±5) were scanned on both RF coils using the same acquisition protocol. Written informed consent was obtained from all subjects for an experimental protocol approved by the institutional review board. Extra padding with foam cushions was used for head immobilization. To avoid any possible bias, the total number of subjects starting the experiment with any given coil was kept equal in the study. This was achieved by counterbalancing the type of coil that the subject starts

and ends the session with, as data from both coils were acquired during the same imaging session. All subjects were asked to relax while in the scanner with their eyes closed, and instructed not to fall asleep. Automatic slice prescription, based on alignment of localizer scans to a multi-subject atlas (van der Kouwe et al., 2005), was used to achieve a consistent slice prescription across the two imaging experiments with the different RF coils. Given that the two coils vary in size, with the 32Ch being smaller and tighter fit, subject positioning could not be identical in the two coils, however we ensured consistent subject positioning within each coil. Specifically, we used similar under-head padding and foam cushions laterally and on top of the head (posterior of the coil) to minimize motion and to ensure each subject was positioned comfortably in the head coils. The mean obliquing parameters across subjects were T>C -19.6±6° >S 1±1.9° for the 12Ch coil, and T>C -18.3±6.5° >S 1.6±1.5° for the 32Ch coil, where T, C, and S denote Transverse, Coronal and Sagittal planes respectively; there was no significant difference in these parameters between the two coils.

Resting-state time-series were acquired using a single-shot gradient echo EPI sequence. At the beginning of each EPI acquisition, two "dummy" scans were acquired and discarded to allow longitudinal magnetization to reach equilibrium. Full head coverage was achieved with sixty-seven 2mm thick interleaved slices with orientation parallel to the anterior commissure – posterior commissure (AC-PC) plane. The imaging parameters were TR=6000 ms, TE=30 ms, flip angle=90°, in-plane spatial resolution of 2 mm x 2 mm and 62 time-points. Each resting scan lasted 6 minutes and 24 seconds. The TR was chosen to be 6 s in this study in order to achieve full-brain coverage at the given resolution of 2mm isotropic voxel size (without utilizing parallel imaging). Full brain coverage was essential in order to map global resting state networks, e.g. Default Mode Network. Array data was combined with the manufacturer's Sum-of-Squares

online reconstruction method. Additionally, a 3D high-resolution T_1-weighted structural scan was collected using an MP-RAGE sequence with voxel size = 1.3x1x1.3 mm^3, other acquisition parameters were: TR/TE/TI/FA=2530 ms/3.39 ms/1100 ms/7°. Additionally, to demonstrate the effect of coil geometry/design and the coil sensitivity profile on the various brain regions, proton density weighted gradient echo images were acquired from one subject in both coils at the same scanning session. Acquisition parameters were: TR/TE/FA = 30ms/6ms/30°, Matrix: 192×192, Field-of-View: 170×170 mm^2, slice thickness: 7 mm, bandwidth = 200 Hz/Pixel. Noise data was also acquired with this acquisition scheme, but with 0V RF excitation.

2.2.2 Data Analysis

The resting state data were pre-processed with standard fMRI pre-processing steps using SPM8, (fil.ion.ucl.ac.uk/spm/software/spm8/) (Friston, 2007b), including: *i*) a six parameter rigid body transformation to account for head motion, and perform image realignment, *ii*) slice-time correction to account for the interleaved slice acquisition, *iii*) normalization using a voxel size of 2x2x2 mm^3 and the EPI template provided with SPM8 to allow comparison between subjects, and, *iv*) smoothing with 3-mm full-width-half-maximum (FWHM) Gaussian kernel. T_1-weighted structural images were segmented to grey matter (GM), white matter (WM) and CSF masks using the segmentation routine in SPM8 (Ashburner and Friston, 2005). The original structural image and the segmented images were also normalized using a voxel size of 1x1x1 mm^3 and the T_1-weighted structural template provided with SPM8. Subject motion was evaluated with in-house custom software (nitrc.org/projects/artifact_detect/). At a motion threshold of 0.4mm, there were a total of 21 outliers in the 12Ch data set and 17 in the 32Ch data set (16 subjects per group). Since there were no significant differences in the mean number of outliers between 12Ch and 32Ch coils, nuisance regression of motion outliers was not carried out. Additionally, there

was no significant difference (p=0.37) in the mean motion parameters between the 12Ch coil (mean motion = 0.49±0.41) and the 32Ch coil (mean motion = 0.38±0.23).

The SNR maps were calculated following the methodology from Kellman and McVeigh (Kellman and McVeigh, 2005). Noise correlations coefficients matrices were calculated from the noise only (RF=0V) acquisitions.

Brodmann Area	x y z	Brain Region
	DMN	
30	0 -52 27	Posterior Cingulate Cortex (PCC)
8	-1 54 27	medial Pre-Frontal Cortex (mPFC)
39	-46 -66 30	left Lateral Parietal Cortex (LPC)
39	49 -63 33	right LPC
20	-61 -24 -9	left Inferior Temporal (IT)
20	58 -24 -9	right IT
-	0 -12 9	medial Dorsal Thalamus (mDT)
-	-25 -81 -33	left Posterior Cerebellum (PC)
-	25 -81 -33	right PC
	HCMN	
27	-21 -25 -14	left Hippocampal Formation (HF)
27	24 -19 -21	right HF
8	0 51 -7	ventro-medial Pre-Frontal Cortex (vmPFC)
30	1 -55 15	PCC
40	-47 -71 29	left posterior Inferior Parietal Lobule (IPL)
40	50 -64 27	right posterior IPL
	DAN	
6	-29 -9 54	left Frontal Eye Field (FEF)
6	29 -9 54	right FEF
7	-26 -66 48	left posterior Intraparietal sulcus (IPS)
7	26 -66 48	right posterior IPS
40	-44 -39 45	left anterior IPS
40	41 -39 45	right anterior IPS
21	-50 -66 -6	left Middle Temporal (MT)
21	53 -63 -6	right MT
	ECN	
8	0 24 46	dorsal mPFC
10	-44 45 0	left anterior PFC
10	44 45 0	right anterior PFC
40	-50 -51 45	left Superior Parietal Cortex (SPC)
40	50 -51 45	right SPC
	SN	
32	0 21 36	dorsal Anterior Cingulate Cortex (ACC)
10	-35 45, 30	left anterior PFC
10	32 45 30	right anterior PFC
13	-41 3 6	left Insula
13	41 3 6	right Insula
40	-62 -45 30	left LPC
40	62 -45 30	right LPC

Table 2.1: Peak foci of seed regions for all networks.

2.2.2.1 First-Level Connectivity Analyses

Functional connectivity analysis was performed using both seed-based and graph-theory approaches with MATLAB (MathWorks, Natick, MA) based custom software package: CONN (Whitfield-Gabrieli and Nieto Castanon, 2012). For seed-based analysis, sources will be defined as multiple seeds corresponding to the pre-defined seed regions for: (*i*) DMN and HCMN, (*ii*) DAN, (*iii*) ECN and (*iv*) SN. All seeds were independent of our data and were generated using WFU_PickAtlas, (nitrc.org/projects/wfu_pickatlas) (Maldjian et al., 2004; Maldjian et al., 2003). Seeds for DMN, DAN, ECN and SN were chosen to be 10-mm spheres centered on previously published foci (Zhang and Raichle, 2010), while HCMN seeds were chosen to be 12.5-mm spheres centered at coordinates provided by the literature (Vincent et al., 2008). Detailed description of the seed regions used are given in Table 2.1. For the subcortical (basal ganglia) network, the sources were anatomical ROIs corresponding to: *(i)* thalamus, *(ii)* striatum (caudate and putamen), *(iii)* globus pallidus (medial and lateral), *(iv)* substantia nigra and *(v)* subthalamic nucleus, derived from WFU_PickAtlas. For graph-theory based analyses all 84 Brodmann areas, anatomically defined from the Talairach Daemon database atlas (Lancaster et al., 2000), were chosen as sources.

The seed time-series went through temporal band-pass filtering ($0.008 < f < 0.09$ Hz). Instead of removing the average signal over all voxels of the brain by global signal regression, contributions from non-neuronal sources, such as WM and CSF were considered as noise, the principal components of which were estimated and removed using, aCompcor (anatomical component based noise correction method) (Behzadi et al., 2007). The optimal configuration of the aCompCor approach (Chai et al., 2011) as applied in the CONN toolbox (Whitfield-Gabrieli

and Nieto Castanon, 2012) was followed. In addition, the six motion (3-rotation and 3-translation) parameters were also regressed out. For quality control purposes, it was ensured that the histogram plot of voxel-to-voxel connectivity (r value) appear approximately centered to the mean for each subject after confound removal. Correlation maps were generated by extracting the residual BOLD time-course from the seeds, followed by computing Pearson's correlation coefficients between the seed time-course and the time-courses of all other voxels. Correlation coefficients were converted to z- scores using Fisher's r-to-z transform to allow for second-level General Linear Model (GLM) analyses. Images from the first-level results (correlation maps and z-maps) provide the seed-to-voxel connectivity maps for each selected source for each subject and for each condition (one per subject/condition/source combination).

2.2.2.2 Second-Level Connectivity Analyses

For both seed-based and graph-theory-based methods, we first performed within- and between-group analysis of full data sets from 32Ch and 12Ch coils. $32Ch_{full}$ and $12Ch_{full}$ refer to "full-length" acquisitions of 6min and 24 s with 62 time-points. In addition, scan time reduction was evaluated by estimating the $32Ch_{half}$ vs. $12Ch_{full}$ contrast (within- and between-group analysis) to examine if sufficient signal power is held by the 32Ch data in the shorter run; $32Ch_{half}$ for "half-length" acquisition with 31 time-points. The outcome of GLM analyses performed at this level was the within-subjects linear combination of effects specified by the *sources* as contrasts, and applied to the first-level connectivity-measure volumes (for the seed-to-voxel analyses). For within-group comparisons of seed-based analyses, whole-brain False Discovery Rate (FDR) corrected threshold of $p<0.05$ ($p_{FDR\text{-}corr}<0.05$) was used to identify areas of significant functional connectivity. For between-group comparisons of task-positive and task negative networks, statistical analysis was performed using a cluster-defining voxel-wise height

threshold of p<0.01 (uncorrected). Since subcortical regions are noisier compared to cortical regions, a whole-brain $p_{FDR\text{-}corr}$<0.05 was used for between-group comparisons. For all the networks, significant clusters were identified with an extent threshold of whole-brain Family Wise Error (FWE)-corrected p<0.05 ($p_{FWE\text{-}corr}$<0.05).

For the graph-theory based analysis [see (Bullmore and Sporns, 2009) for review], we chose ***Global Efficiency, Local Efficiency*** and ***Cost.*** These metrics are particularly relevant for probing brain networks because of their computational validity for unconnected and weighted graphs (Achard and Bullmore, 2007). *Global efficiency* of a node is the average inverse shortest-path distance between a given node and all other nodes in the network (targets). *Local efficiency* of a node is the average inverse shortest-path distance among the target nodes connected to a given node. *Cost* or *Degree* of a node is the proportion of nodes connected to a given node. Equivalent network-level measure of these metrics is the average (across all nodes in the network) of their corresponding node-specific measures. The computational formulas are given below (in Equations 2.1, 2.2 and 2.3) where |G|, E and C denote the number of nodes (n) in graph G, efficiency and cost respectively.

Global Efficiency:

$$E^{global}(G) = \frac{1}{|G|}.\sum_{n\in G} E_n^{global}(G) \tag{2.1}$$

Local Efficiency:

$$E^{local}(G) = \frac{1}{|G|}.\sum_{n\in G} E_n^{local}(G) \tag{2.2}$$

Cost:

$$C(G) = \frac{1}{|G|}.\sum_{n\in G} C_n(G) \tag{2.3}$$

Global Efficiency of a node is the 'centrality' of the nodes' connectivity, i.e., the extent of connectivity of the node with the rest of the network, whereas on the network level, it serves as a measure of the extent of centrality as well as the "efficiency" of this connectivity (nodes with higher global efficiency are "better connected"). In contrary, *Local Efficiency* of a node represents the 'locality' of the nodes' connectivity, i.e., the extent of connectivity of the node with its neighbors (as well as the "redundancy" or fault tolerance of the node), whereas on the network level, it provides a measure of the extent of locality i.e., nodes with high local efficiency are connected to neighbors that form a strong or well-connected local network, while nodes with low local efficiency are connected to neighbors that are sparsely connected or distant to each other. Global efficiency typically reflects the relevance of long-range connections (meaning higher global efficiency = better long-range connectivity); where as local efficiency is reflective of the relative relevance of short-range connections in the overall network connectivity (meaning higher local efficiency = better short-range connectivity). Finally, *Cost* of a node can be interpreted as the strength of connectivity of a node, whereas on the network level, cost indicates hypo/hyper connectivity in the overall network (e.g., higher cost=overall hyper-connectivity). The approach used is part of the CONN toolbox and has been described in great detail in a recently published manuscript (Whitfield-Gabrieli and Nieto Castanon, 2012).

To contrast network-level estimations of global efficiency, local efficiency and cost, a fixed percentile cost threshold (top 15% of ROI-to-ROI connectivity) was used to calculate connectivity (adjacency) matrix (within the 84 Brodmann area ROIs), followed by a threshold of $p_{FDR\text{-}corr}<0.05$, for both within- and between-group comparisons.

2.3 Results

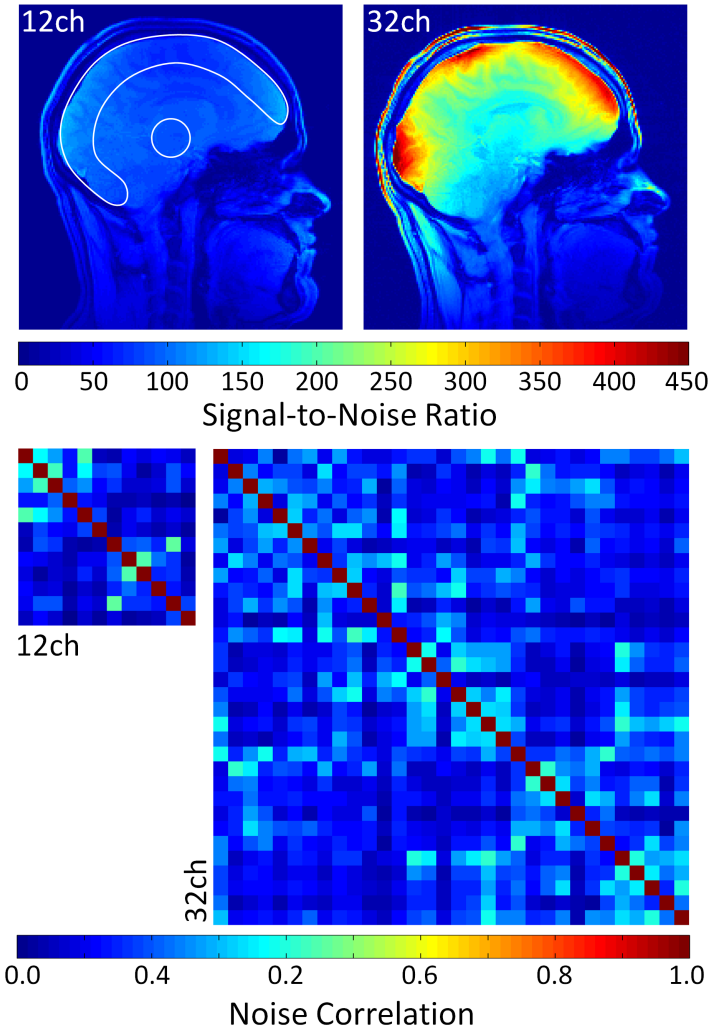

Figure 2.1: Pixel-wise SNR maps and noise correlation matrices from the 12Ch and 32Ch array coils. The 32Ch coil outperforms the 12Ch coil by a factor of 2.3x averaged over the given signal area. SNR from the peripheral cortex and the central brain region were obtained from the labeled Regions-of-Interest. The 32ch coil shows a 1.25-fold and 2.7-fold SNR improvement in the brain center and cortex, respectively. SNR increase in the corpus callosum region is 1.4-fold. SNR gain of the 32Ch coil can be attributed to both higher channel count and smaller helmet size. The 12Ch and 32Ch coil show average noise correlation (bottom row) of 12.3% and 9.7%, respectively.

Figure 2.1 shows the coils' sensitivity on a human subject in terms of pixel-wise image SNR maps (top row) as well as the noise correlation matrices across individual elements from the 12Ch and 32Ch array coils (bottom row). Data was acquired from the same subject in both coils at the same scanning session. The comparison reveals that the 32Ch array outperforms the 12Ch coil by a factor of 2.3x averaged over the given signal area. The peripheral cortex, corpus

callosum, and midbrain (thalamic) regions show SNR improvements by a factor of 2.7x, 1.4x, and 1.25x respectively, exhibiting the increased sensitivity offered by the 32Ch coil not only at the cortex, but also at sub-cortical regions and deeper structures. The 12Ch and 32Ch coil show average noise correlation of 12.3% and 9.7%, respectively. Some of the correlation is likely due to remaining inductive coupling, but some is due to shared resistance through the sample.

2.3.1 Seed-based Analysis

Figure 2.2 shows group-level results for the task negative default networks (DMN and HCMN) from the 32Ch and 12Ch array coils. Connections in all the seeds in the DMN (Figure 2.2 A) and HCMN (Figure 2.2 B) are significantly stronger in the 32Ch data set. Connections in left and right Inferior Temporal Gyrus (ITG) extending to left and right Parahippocampal Gyrus (PHG), Superior Parietal Cortex (SPC) and Middle Temporal Gyrus (MTG) are more significant for DMN in the $32Ch_{full} > 12Ch_{full}$ comparison (Table 2.2). Even with half the data set (Table 2.3), connections within the Superior Frontal Gyrus (SFG), Superior Parietal Lobule (SPL) and Superior Temporal Gyrus (STG) were revealed with the 32Ch coil. For HCMN, connections in the left and right Secondary Visual Cortex (SVC), Orbitofrontal Cortex (OFC) and left and right MTG were significantly more pronounced in the $32Ch_{full} > 12Ch_{full}$ comparison (Figure 2.4 A). Medial Pre-frontal Cortex (PFC) was significant even with $32Ch_{half} > 12Ch_{full}$ contrast (Table 2.3).

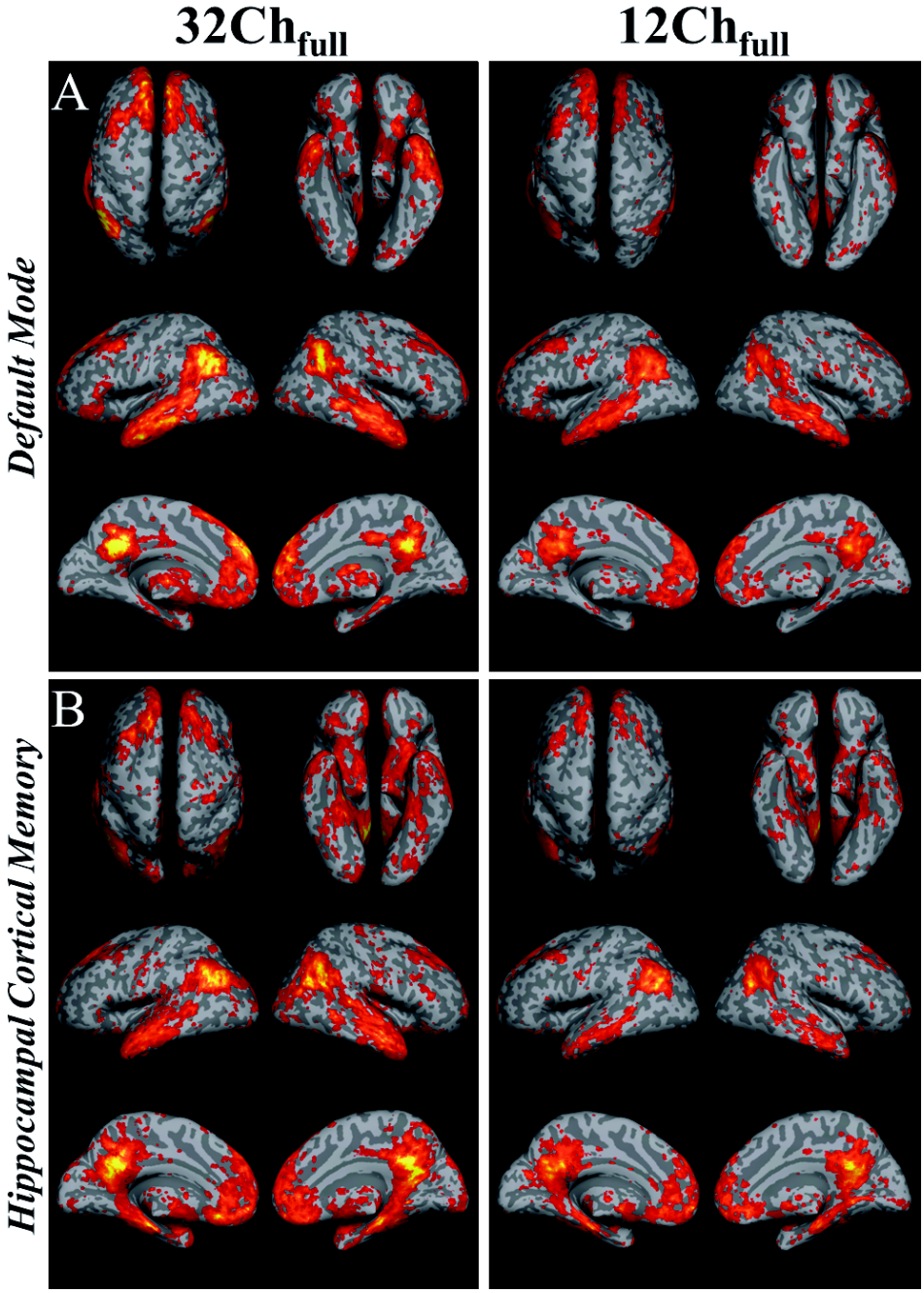

Figure 2.2: Statistical functional connectivity maps for the task negative networks from 32Ch and 12Ch coils (second-level analysis, n=16 per group; whole-brain $p_{FDR\text{-}corr}<0.05$).

Group-level results for the task positive networks (DAN, ECN and SN) from the 32Ch and 12Ch coils are shown in Figure 2.3. The 12Ch coil only revealed a small subset of the functional connectivity in DAN (Figure 2.3 A). Connections in dorso-lateral PFC (DLPFC), left

and right fusiform gyrus, anterior PFC (APFC), ITG and SPL were significantly stronger in the 32Ch data set (Table 2.2). $32Ch_{half} > 12Ch_{full}$ comparison (Table 2.3) revealed DLPFC, APFC, premotor cortex and SPL.

Brain Region	Brodmann Area	Peak cluster	Voxels per cluster	T_{max}
	DMN			
left Inferior Temporal Gyrus (ITG)	BA 20	-48 -6 -38	1016	6.35
right Superior Parietal Cortex (SPC)	BA 40	38 -50 28	161	5.32
right Secondary Visual Cortex (SVC)	BA 18	34 -76 -20	212	4.85
right ITG	BA 20	40 -2 -48	244	4.38
right Middle Temporal Gyrus (MTG)	BA 21	46 -4 -20	160	3.89
	HCMN			
left SVC	BA 18	-16 -100 18	255	6.51
right MTG	BA 21	56 -12 6	614	5.15
Orbitofrontal Cortex (OFC)	BA 11	4 24 -22	263	4.99
left MTG	BA 21	-56 -18 8	207	4.96
right SVC	BA 18	24 -98 12	223	4.34
	DAN			
right Dorso Lateral Pre-Frontal Cortex (DLPFC)	BA 9	44 26 38	212	5.26
right Fusiform Gyrus	BA 37	48 -50 -14	309	5.09
right anterior Pre-Frontal Cortex (PFC)	BA 10	24 66 -10	144	4.88
left Fusiform Gyrus	BA 37	-50 -56 -2	232	4.66
left ITG	BA 20	-58 -32 -20	151	4.45
left Superior Parietal Lobule (SPL)	BA 7	-16 -48 50	114	4.06
	ECN			
right Superior Frontal Gyrus	BA 8	40 26 38	439	8.73
left MTG	BA 21	-58 -38 -8	285	5.32
right MTG	BA 21	56 -44 0	262	4.88
left DLPFC	BA 9	-36 2 32	225	4.76
left SPC	BA 40	-52 -38 52	112	4.71
left anterior PFC	BA 10	-20 62 10	254	4.50
right anterior PFC	BA 10	36 40 2	138	4.33
Premotor Cortex	BA 6	20 14 56	128	3.72
	SN			
left Insular Cortex	BA 13	-34 6 -2	917	7.07
right Insular Cortex	BA 13	32 16 6	1243	6.15
dorsal Anterior Cingulate Cortex	BA 32	-4 26 24	920	5.51
right anterior PFC	BA 10	34 3 8	143	4.91
left DLPFC	BA 9	-26 38 20	507	4.86
right DLPFC	BA 9	32 46 36	483	4.81
left DLPFC	BA 9	-46 2 20	112	4.31
left SPC	BA 40	-58 -38 40	182	4.03

Table 2.2: Positively correlated brain regions for $32Ch_{full} > 12Ch_{full}$ contrast (second-level group analysis, n = 16 per group; cluster-level $p_{FWE\text{-}corr}<0.05$; height threshold: T = 2.46); opposite contrast was not significant.

Figure 2.3 B shows the functional connectivity correlation maps generated at the second level for ECN. The $32Ch_{full} > 12Ch_{full}$ comparison (Table 2.2) revealed significant differences in SFG, left and right MTG, DLPFC, SPC, left and right APFC and premotor cortex. The contrast

$32Ch_{half}$ > $12Ch_{full}$ (Table 2.3) also revealed significant differences, primarily in APFC. Entire network (dorsal medial PFC, left and right APFC and left and right SPC) was significantly stronger with half the data set from the 32Ch coil (Figure 2.4 B).

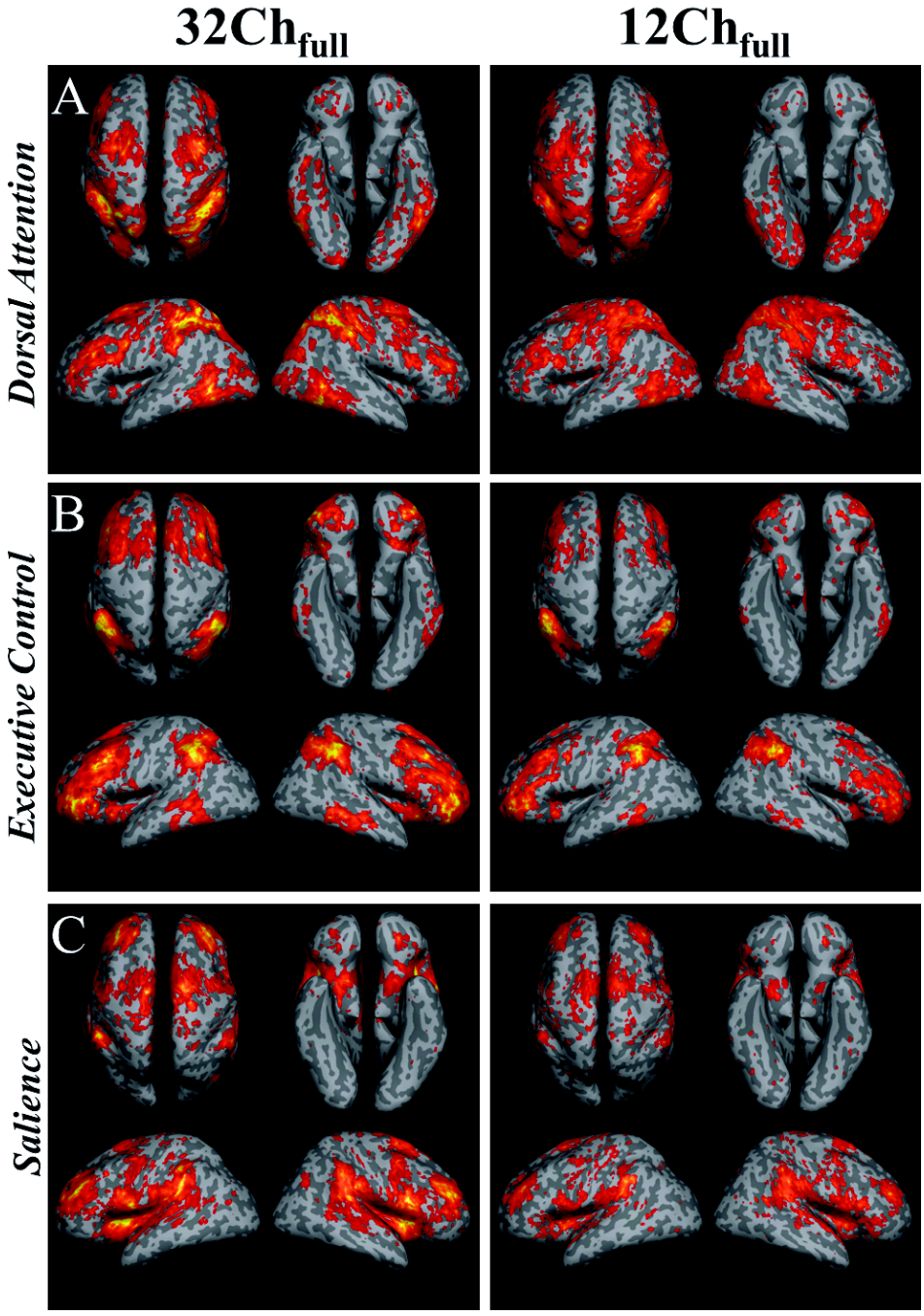

Figure 2.3: Statistical functional connectivity maps for the task positive networks from 32Ch and 12Ch coils (second-level analysis, n=16 per group; whole-brain $p_{FDR\text{-}corr}$<0.05).

Similarly to all the above-mentioned networks, the second level analysis for SN (Figure 2.3 C) revealed only a smaller subset of the network for the 12Ch coil. Connections in left and right insular cortex were remarkably stronger with the 32Ch (both full and half data sets) in comparison to 12Ch coil (Table 2.2). In addition, $32Ch_{full} > 12Ch_{full}$ comparison revealed dorsal Anterior Cingulate Cortex (ACC), APFC, left and right DLPFC, and SPC (Table 2.3).

Brain Region	Brodmann Area	Peak cluster	Voxels per cluster	T_{max}
	DMN			
Superior Frontal Gyrus (SFG)	BA 8	14 40 44	98	4.72
Superior Parietal Lobule (SPL)	BA 7	34 -64 50	91	4.43
left Superior Temporal Gyrus	BA 22	-54 -34 -2	106	4.16
	HCMN			
Premotor Cortex	BA 6	32 -6 54	95	5.08
Orbitofrontal Cortex (OFC)	BA 11	-6 16 -24	337	4.93
SFG	BA 8	0 34 40	480	4.72
left Dorsolateral PFC (DLPFC)	BA 46	-44 32 10	102	4.56
Dorsal Anterior Cingulate Cortex	BA 32	6 34 8	153	4.48
right SPL	BA 7	42 -64 48	113	4.44
right DLPFC	BA 46	44 46 12	130	4.24
	DAN			
right DLPFC	BA 9	48 36 26	107	6.41
right anterior Pre-Frontal Cortex (PFC)	BA 10	38 56 14	210	5.12
Premotor Cortex	BA 6	60 -14 16	116	4.83
left SPL	BA 7	-24 -54 48	102	4.67
	ECN			
right Inferior Temporal Gyrus	BA 20	54 -22 -18	127	6.78
right anterior PFC	BA 10	40 26 36	789	6.76
right Insular Cortex	BA 13	52 -12 2	175	5.69
right anterior PFC	BA 10	34 52 -6	521	5.20
right Superior Parietal Cortex (SPC)	BA 40	52 -52 50	286	5.14
left SFG	BA 8	-8 28 46	245	5.10
left DLPFC	BA 9	-40 28 26	94	4.91
right Fusiform Gyrus	BA 37	54 -44 -6	93	4.90
left anterior PFC	BA 10	-4 46 8	130	4.22
left SPC	BA 40	-36 -62 50	147	4.12
	SN			
right Insular Cortex	BA 13	36 -4 -6	146	6.30
left Insular Cortex	BA 13	-32 -4 -12	215	5.82
SPL	BA 7	-2 -66 32	170	4.31

Table 2.3: Positively correlated brain regions for $32Ch_{half} > 12Ch_{full}$ contrast (second-level group analysis, n = 16 per group; cluster-level $p_{FWE\text{-}corr}<0.05$; height threshold: T = 2.46); opposite contrast was not significant.

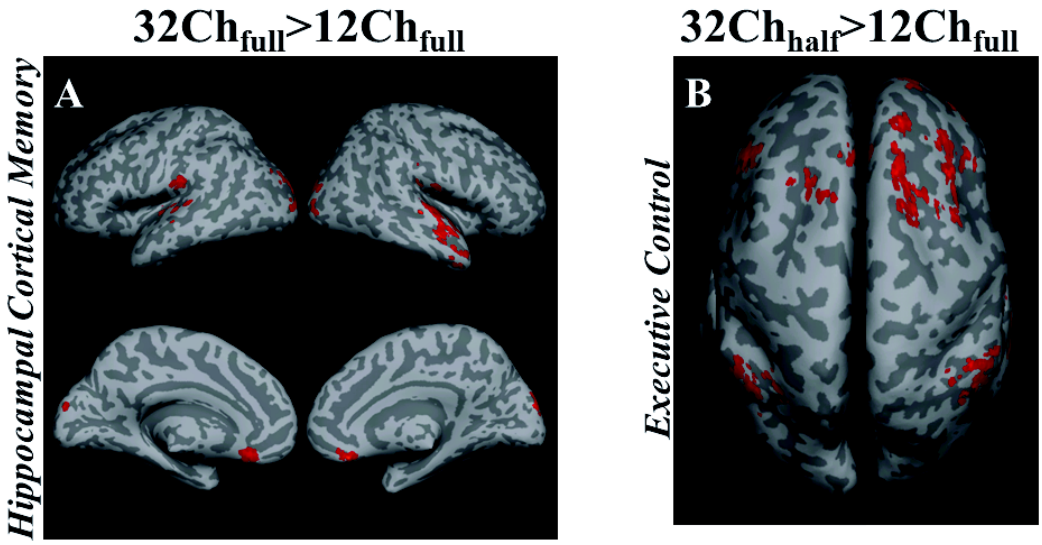

Figure 2.4: Representative examples from a task negative and task positive resting state network for between group comparisons from (A) $32Ch_{full} > 12Ch_{full}$ and (B) $32Ch_{half} > 12Ch_{full}$ contrasts (second-level analysis, n=16 per group; cluster-level $p_{FWE\text{-}corr}<0.05$; height threshold: T = 2.46). (A) Connections in left and right temporal gyrii and medial prefrontal cortices of the default network are revealed significantly more with 32Ch coil. (B) Entire ECN (dorsal mPFC, left and right anterior pre-frontal cortices and left and right superior parietal cortices) is revealed significantly more with half the data set from 32Ch coil.

For all the resting state networks studied above, both $12Ch_{full} > 32Ch_{full}$ and $12Ch_{full} > 32Ch_{half}$ contrasts were not significant.

To evaluate the sensitivity of the coils in deeper brain structures, the subcortical network of basal ganglia was explored. Group level results based on seed-to-voxel analysis demonstrated stronger functional connectivity in all the sub-cortical ROIs with 32Ch coil (Figure 2.5). The $32Ch_{full} > 12Ch_{full}$ comparison (whole-brain $p_{FDR\text{-}corr}<0.05$, cluster-level $p_{FWE\text{-}corr}<0.05$) revealed significantly stronger connections in bilateral pallidum, bilateral putamen, left precentral gyrus (BA 6) and STG (BA 22). ROI-to-ROI connectivity analysis for within-group comparisons ($p_{FDR\text{-}corr}<0.05$) revealed several interesting findings: 1) With thalamus as seed ROI, 12Ch group failed to identify functional connectivity from relatively smaller structures such as substantia nigra and subthalamic nucleus; this was also the case when medial globus pallidus was chosen as the ROI; 2) With caudate (part of striatum) as seed ROI, correlations with medial globus pallidus

was detected only by the 32Ch group, and 3) With lateral globus pallidus as seed ROI, the T-scores for positive correlations from substantia nigra and subthalamic nucleus were: 6.27 and 5.67 with 32Ch coil; and 2.26 and 2.17 with the 12Ch coil.

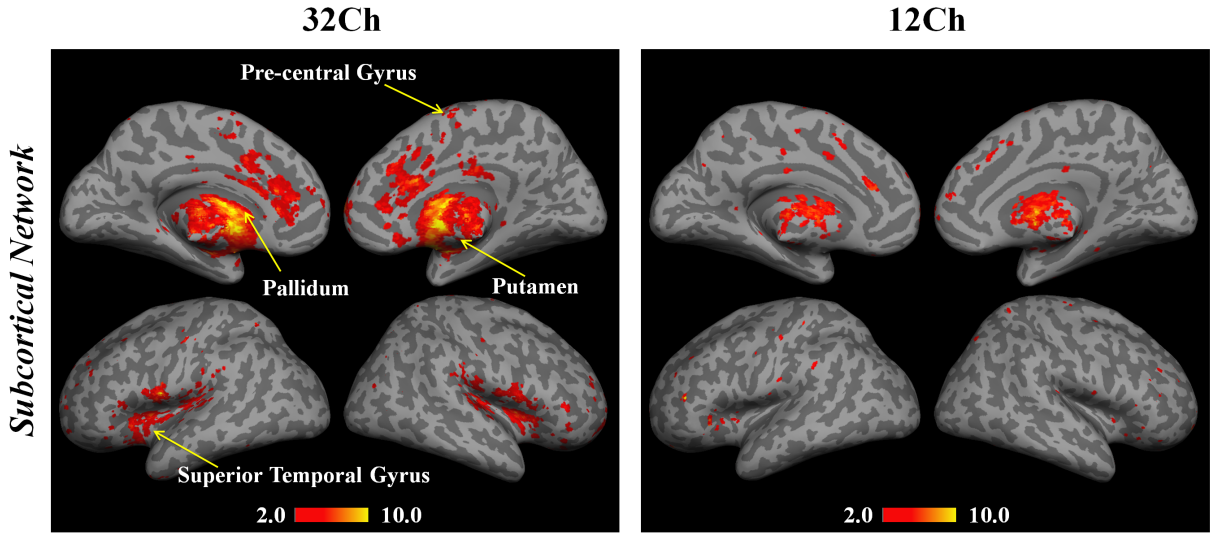

Figure 2.5: Statistical functional connectivity maps for the subcortical network from 32Ch and 12Ch coils (full data sets, second-level analysis, n=16 per group; whole-brain $p_{FDR\text{-}corr}<0.05$). Yellow arrows indicate regions that are significantly different in $32Ch_{full} > 12Ch_{full}$ contrast (whole-brain $p_{FDR\text{-}corr}<0.05$, cluster-level $p_{FWE\text{-}corr}<0.05$).

2.3.2 Graph-theory Based Analysis

Consistent with the small-world behavior of brain networks reported before (Achard and Bullmore, 2007), graph-theory analyses revealed monotonic increases in global and local efficiency as a function of cost in all brain networks (Figure 2.6). As shown in Figure 2.6 top row, the random graph had higher global efficiency than the lattice and vice versa for local efficiency, for costs (K) in the range $0 \leq K \leq 0.5$. Brain networks (solid black line pertaining to our data represents data from all subjects for both 12Ch and 32Ch coils), however in the cost range of $0.05 \leq K \leq 0.34$, had global efficiency greater than the lattice but less than the random graph, and local efficiency greater than random but less than lattice (Figure 2.6, bottom row). We therefore chose a cost threshold of 0.15 for our analyses.

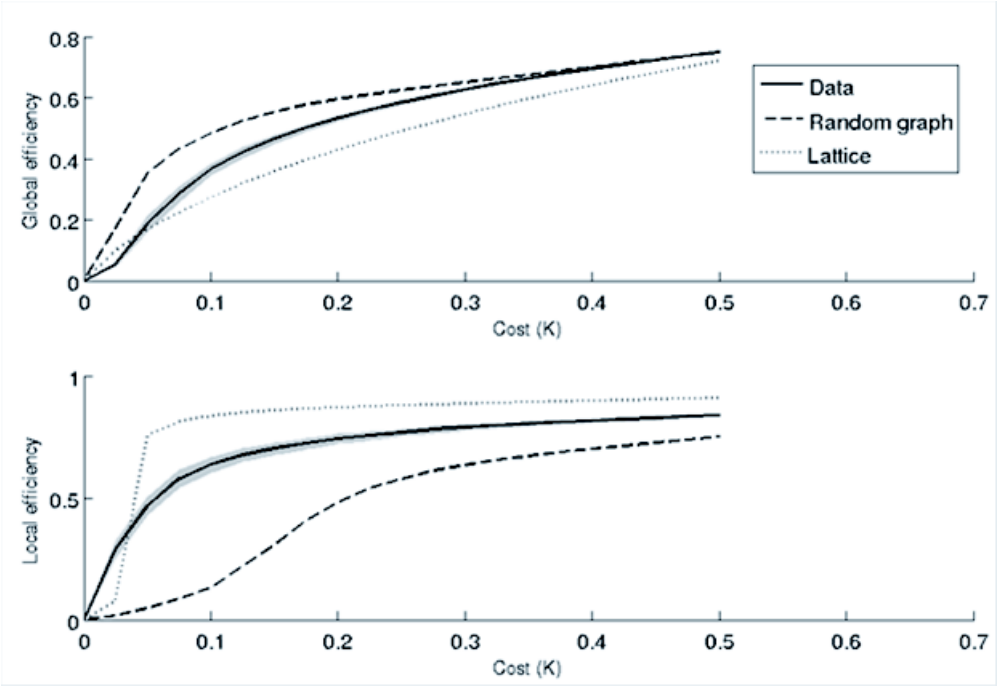

Figure 2.6: Global and local efficiency (y-axis) as a function of cost (x-axis) for a random graph, a regular lattice and brain networks. On average, over all subjects in both the 12Ch and 32Ch groups, brain networks have efficiency curves located between the limiting cases of random and lattice topology. Solid black line represents data from all subjects for both the 12Ch and 32Ch coils.

In the $32Ch_{full} > 12Ch_{full}$ contrast, analysis of global efficiency ($p_{FDR\text{-}corr}<0.05$) only left and right ACC (BA 33) surpassed the top 15% ROI-to-ROI connectivity (cost threshold of 0.15) from the network of all sources (84 Brodmann areas). Results from network level analysis of cost are shown in Figure 2.7. Left and right ACC, left and right anterior entorhinal cortex (BA 34) and right perirhinal cortex (BA 35) surpassed the threshold ($p_{FDR\text{-}corr}<0.05$) for $32Ch_{full} > 12Ch_{full}$ contrast (Figure 2.7 C). Even with half the data set from 32Ch coil, analysis of cost ($p_{FDR\text{-}corr}<0.05$) in the $32Ch_{half} > 12Ch_{full}$ contrast revealed bilateral ACC. Analysis of local efficiency ($p_{FDR\text{-}corr}<0.05$) revealed right ACC and left PHG (BA 36). The opposite contrasts ($12Ch_{full} > 32Ch_{full}$ and $12Ch_{full} > 32Ch_{half}$) were not significant for all three measures. Global and local efficiency comparisons of full and half data sets from 32Ch, and full data sets from 12Ch coil at the cost threshold of 0.15 are summarized in Table 2.4.

Coil	Global Efficiency	Local Efficiency
$32Ch_{full}$	0.471	0.717
$32Ch_{half}$	0.455	0.697
$12Ch_{full}$	0.459	0.688
p_{FDR} ($32Ch_{full}$ > $12Ch_{full}$)	0.056	0.034
p_{FDR} ($12Ch_{full}$ > $32Ch_{full}$)	n.s	n.s

Table 2.4: Global and local efficiency comparisons of 32Ch and 12Ch coils (graph theory analysis), for the top 15% ROI-to-ROI connectivity ($p_{FDR\text{-}corr}$<0.05), from from all Brodmann areas (number of nodes = 84, 16 subjects per group).

T-values from $32Ch_{full}$, $12Ch_{full}$, and $32Ch_{full}$ > $12Ch_{full}$ comparisons from the network level analysis of cost (depicted in Figure 2.7) for the top 15% ROI-to-ROI connectivity ($p_{FDR\text{-}corr}$<0.05) from all Brodmann areas (number of nodes = 84, 16 subjects per group) is provided in Table 2.5. Brain regions provided in column 1, correspond to the ROIs represented as circles in Figure 2.7 C ($32Ch_{full}$ > $12Ch_{full}$ comparison). Precisely, these are the brain regions that surpassed the threshold ($p_{FDR\text{-}corr}$<0.05) for $32Ch_{full}$ > $12Ch_{full}$ contrast during the network-level analysis of cost.

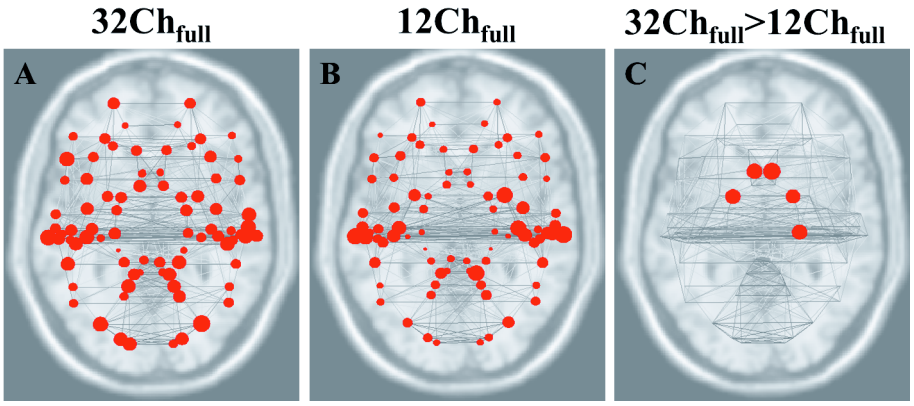

Figure 2.7: Graph visualization of the network-level analysis of cost for the top 15% ROI-to-ROI connectivity ($p_{FDR\text{-}corr}$<0.05) from all Brodmann areas (number of nodes = 84,16 subjects per group). Circle-sizes represent T-values.

Brain Region	T-scores		
	32Ch	***12Ch***	***32Ch>12Ch***
left Anterior Entorhinal Cortex	9.73	6.21	3.18
right Anterior Entorhinal Cortex	9.68	8.82	2.99
right Perirhinal Cortex	8.45	5.83	3.17
right Anterior Cingulate Cortex (ACC)	6.01	3.31	3.58
left ACC	4.70	3.57	3.26

Table 2.5: T-values from $32Ch_{full}$, $12Ch_{full}$, and $32Ch_{full} > 12Ch_{full}$ comparisons from the network level analysis of cost (depicted in Figure 2.7) for the top 15% ROI-to-ROI connectivity ($p_{FDR\text{-}corr}<0.05$) from all Brodmann areas (number of nodes = 84, 16 subjects per group). Brain regions provided in column 1, correspond to the ROIs represented as circles in Figure 2.7 C ($32Ch_{full} > 12Ch_{full}$ comparison). Precisely, these are the brain regions that surpassed the threshold ($p_{FDR\text{-}corr}<0.05$) for $32Ch_{full} > 12Ch_{full}$ contrast during the network-level analysis of cost.

2.4 Discussion

Multichannel arrays offer close head-fittings, impressive increases in the image SNR, especially in cortical areas, and remarkable accelerated imaging capabilities. Because of these advantages, multichannel array coils have recently become widely available as experimental devices (Keil et al., 2011; Keil et al., 2012; Wiggins et al., 2006) and also as clinical research tools (Knake et al., 2005). In this study, task positive (dorsal attention, executive control and salience), task negative (default mode and hippocampal cortical memory), and subcortical (basal ganglia) resting state networks were assessed to examine whether increases in tSNR with the additive coil sensitivity of a 32Ch brain array can translate to higher functional connectivity detectability when compared to a 12Ch coil. Our findings, from both seed-based and graph-theory-based functional connectivity analyses methods, demonstrated that the 32Ch brain array revealed stronger connections ($32Ch_{full} > 12Ch_{full}$ contrast) in all the resting state networks studied. Furthermore, precise localization of functional connectivity mapping was also observed using the 32Ch coil, when fMRI time-series acquisition time was reduced to half of its original duration (~3min vs. 6min scan).

The increased SNR capabilities of 32Ch coil in combination with the high-resolution acquisition scheme enabled us to identify the resting state networks at the group level (16 subjects) in greater detail compared to the 12Ch coil. The core of the default mode network according to the literature is formed by PCC, MPFC, left and right LPC and left and right inferior temporal cortices (Fox et al., 2005). The fact that the Inferior Temporal Gyrus was detected to a significantly stronger extend by the 32Ch coil, reflects one of the major limitations of 12Ch coil in terms of SNR at higher resolution acquisitions. Furthermore, connections from relatively smaller brain structures, like PHG, which are not typically identified even at group level by 12Ch coil, was detected by the 32Ch coil in our group data. This was particularly accurate in the HCMN comparison between the two coils. Significantly better detection of connections between hippocampus and orbitofrontal gyrus, offer a clear advantage for using 32Ch coil in studies involving hippocampal-orbitofrontal connectivity, particularly in the context of epilepsy (Catenoix et al., 2005). For the Dorsal Attention Network (DAN), at which FEF, IPS and MTG comprise the core signal components (Fox et al., 2005), functional connectivity was extremely weak, particularly in the frontal and parietal cortices when the data from the 12Ch coil was used. Core signal components of the Executive Control Network (ECN), IFG, MFG and SFG (Seeley et al., 2007), as well as insula and cingulate cortex, that comprise the Salience Network (SN) (Taylor et al., 2009), were significantly stronger for $32Ch_{full} > 12Ch_{full}$ comparison. Impairments in executive network have been suggested in social anxiety disorders (Qiu et al., 2011), where the 32Ch coil could offer a clear benefit. Right insular cortex even surpassed a much stronger threshold (whole-brain $p_{FDR\text{-}corr}<0.05$) for $32Ch_{full} > 12Ch_{full}$ contrast. This is of particular significance in light of previous research (Sridharan et al., 2008) and more recently in addiction studies (Sutherland et al., 2012), which showed that right-fronto insular

cortex is a network hub that plays a critical role in initiating the spontaneous switching between the task-positive (ECN) and task-negative (DMN) networks (Honey et al., 2007).

To explore further the CNR advantages of the 32Ch we have investigated functional connectivity in the deeper structures of the thalamus and basal ganglia (i.e. sub-cortical network). Between group comparisons ($32Ch_{full} > 12Ch_{full}$) revealed significantly stronger connections in bilateral pallidum, bilateral putamen, left pre-central gyrus, superior temporal gyrus, as well as within the basal ganglia structures, consistent with recent reports using 16Ch coil at 7T (Lenglet et al., 2012). Furthermore, the 12Ch coil failed to identify connections with substantia nigra and subthalamic nucleus, which are relatively smaller structures that are typically excluded from analysis when low-resolution acquisition (3x3x3 mm^3) is employed (Di Martino et al., 2008). This result is in agreement with the SNR performance showing in Figure 2.1, where the 32Ch array outperforms the 12Ch coil in SNR by a factor of 1.25x and 2.7x at the central and peripheral cortex respectively. By increasing the channel count of a head array coil from 12 to 32, an overall 1.8-fold SNR improvement can be expected (Wiesinger et al., 2004). The main SNR gain contribution is expected to occur at the peripheral regions (e.g. brain cortex), while the central SNR will remain relatively the same. However, product available 32Ch head array coils provide a tighter fit compared to dimensionally larger designed 12Ch coils. For the arrays under study in the present work (32Ch and 12Ch coils) since the 32Ch array is also constructed on a tighter fitting helmet than the 12Ch (or most other arrays), it also enjoys a sensitivity benefit from the closer proximity between receive-element and brain. This benefit extends to deep structures as well as superficial cortex. Increases in SNR obtained from 32Ch coils can then be traded off for acquisitions with higher spatial resolution, which becomes particularly important for fMRI.

Graph theory analyses revealed significantly higher overall global efficiency of nodes (i.e. stronger connections) with 32Ch coil compared to 12Ch coil, particularly in ACC. There is converging evidence from recent publications that functional connectivity in ACC changes through brain maturation in healthy subjects (Kelly et al., 2009) and also in ADHD patients (Qiu et al., 2010). Significantly higher local efficiency of PHG revealed by 32Ch coil compared to 12Ch coil showing that this region formed a strong/well-connected network with its neighbors. In the $32Ch_{full} > 12Ch_{full}$ contrast, there is a trend ($p=0.056$) towards higher global efficiency. This could be indicative of the sensitivity of the 32Ch coil to detect long-range connections. In particular, differences in global efficiency between networks are typically related to differences in the amount of long-range connectivity within the network for small-world networks. Similarly, significantly different local efficiency ($p=0.034$) in the $32Ch_{full} > 12Ch_{full}$ contrast indicates the sensitivity of the 32Ch coil to detect short-range connections (because short-range connections are associated to higher local efficiency, i.e., how well are still its neighbors connected if we eliminate this node). Since these two metrics are vital to understanding brain's ability to integrate information at the global level (i.e., functional integration) and cluster level (i.e., functional segregation) (Rubinov and Sporns, 2010), 32Ch coil would prove more beneficial to elucidate the intricacies of brain networks. Cost advantages of 32Ch coil are depicted in Figure 7, which provides a graph visualization of the network-level analysis of cost for the top 15% ROI-to-ROI connectivity ($p_{FDR\text{-}corr}<0.05$) from all Brodmann areas (number of nodes = 84; 16 subjects per group). Network level analysis of cost revealed that connections in ACC are significantly stronger in both $32Ch_{full} > 12Ch_{full}$ and $32Ch_{half} > 12Ch_{full}$ comparisons. Perirhinal, entorhinal, and parahippocampal cortices are part of the medial temporal lobe (MTL) and based on our results, especially from graph-theory analysis, we suggest that 32Ch coil would

be better suited for studies involving MTL pathologies such as Alzheimer's disease and epilepsy. Significantly higher functional connectivity, observed in inferior/medial temporal regions with 32Ch coil, consistently in DMN, HCMN, DAN and ECN reiterates this benefit.

In this study time-series data were acquired in a relatively higher spatial resolution (2x2x2 mm^3) compared to typically employed low resolution (3x3x4 mm^3) in fMRI, based on findings from a recent work (Triantafyllou et al., 2011) which demonstrated that array coils provide biggest increases in tSNR at high spatial resolutions (small voxel size). In our resting state protocol we chose to acquire data at a 2mm isotropic voxel size to utilize the benefits of the multichannel array as well as to increase the spatial specificity and localization of the networks and minimize partial volume effects and physiological noise contamination.

In functional MRI (fMRI) studies, events/blocks are repeated several times so that task related activations are detected more reliably. This often leads to long experiments inducing subject fatigue and/or head motion, the levels of which may confound the results. Moreover, such long experiments might not be feasible on specific subject populations, such as pediatrics or patients. Typically, reduction in scan time is possible only at the expense of SNR, but not necessarily if one could capitalize on the increased sensitivity afforded by multichannel arrays or high magnetic field strength. In this study, we demonstrate that increases in tSNR offered by 32Ch coil can also translate to reductions in scan time, i.e. less number of time points per functional run or ultimately less runs of the same experiment in fMRI. In our resting state experiments, particularly, connections within SFG were significantly stronger in the $32Ch_{half}$ > $12Ch_{full}$ comparison for both DMN and HCMN, as were DLPFC, APFC, premotor cortex and SPL in DAN (task-positive network). Similarly, the ECN and the salience network revealed, within network, significantly strong connections with half the duration of the 32Ch fMRI

acquisition. Similarly, this can also be translated to power calculations for group fMRI studies, (Mumford and Nichols, 2008), by having a lesser sample size or preventing the collection of additional data that will have little impact on power.

The signal dynamic range of the 32Ch receive coil in the brain is approximately twice as that of the 12Ch head coil. This steeply varying spatial sensitivity profile of the small receiver coil elements of the 32Ch array has two important consequences. Firstly, it causes a non-uniform detection sensitivity that spatially modulates the ability to detect BOLD fluctuations. This adds to other sources of BOLD detection variation such as biological effects (differences in CBF and CBV responses and differing hemodynamic response functions) as well as other instrumental effects such as imperfect B_0 shimming (which creates T2* variation and subsequently degrades the optimality of the TE setting). The effect of the coil sensitivity can be easily visualized by creating a tSNR map of the resting brain. Alternatively, the BOLD sensitivity map (Deichmann et al., 2002; Gorno-Tempini et al., 2002) includes this information through the explicit incorporation of the image signal intensity profile.

The most problematic issue concerning the spatially varying reception is the increased sensitivity to motion. Motion effects in resting state have well known detrimental consequences (Power et al., 2012; Satterthwaite et al., 2012; Van Dijk et al., 2012), which are exacerbated when parallel imaging acceleration is used incorporating reference data or coil sensitivity maps taken at the beginning of the scan. Movement then leads to changing levels of residual aliasing in the time-series. Even for non-accelerated imaging, problems derive from the spatially varying signal levels present in an array coil image. Even after perfect rigid-body alignment (motion correction), the signal time-course in a given brain structure remain modulated by the motion of that structure through the steep sensitivity gradient. Motion correction (prospective or

retrospective) brings brain structures into alignment across the time-series but does not alter their intensity changes incurred from movement through the coil profiles of the fixed-position coils. This effect can be partially removed by regression of the residuals of the motion parameters; a step that has been shown to be very successful in removing nuisance variance in ultra-high field array coil data (Hutton et al., 2011). An improved strategy might be to model and remove the expected nuisance intensity changes using the motion parameters and the coil sensitivity map.

As it has been already demonstrated, the achievable SNR improvements of the 32Ch over the 12Ch head coil at the cortex but also at deeper brain areas are due to the increased number of elements and the tight fitting helmet design of the 32Ch array, respectively. However, in practice there are potentially two limitations associated to the tight fitting design; a) not all head sizes fit in the helmet and b) there is no room for the commonly used MRI compatible headphones with big earmuffs. For the later, alternative solutions should be consider, for example inner-ear headphones or ultra-slim earmuffs available in the market.

Chapter 3

Hyper-connectivity of Sub-cortical Resting State Networks in Social Anxiety Disorder

Abstract

Social anxiety disorder related alterations in basal ganglia regions, such as striatum and globus pallidus, though evident from metabolic imaging, remain to be explored using seed-based resting state functional connectivity MRI (fcMRI). Capitalizing on the enhanced sensitivity of a multichannel array coil, we collected high-resolution (2mm isotropic) data from medication naïve patients and healthy control participants. Subcortical resting state networks from structures including the striatum (caudate and putamen), globus pallidus, thalamus, and cerebellum were compared between the two groups. When compared to controls, the caudate seed revealed significantly higher functional connectivity (hyper-connectivity) in the patient group in medial frontal, pre-frontal (anterior and dorso-lateral), orbito-frontal and anterior cingulate cortices, which are regions that are typically associated with emotional processing. In addition, with the putamen seed, the patient data exhibited increased connectivity in the fronto-parietal regions (Executive Control Network) and subgenual cingulate (Affective Network). The globus pallidus seed showed significant increases in connectivity in the patient group, primarily in the precuneus, which is part of the Default Mode Network. Significant hyper-connectivity in the precuneus, interior temporal and parahippocampal cortices was also observed with the thalamus

seed in the patient population, when compared to controls. Seeds from the cerebellum resulted in left lateralized hyper-connectivity with the amygdala in the patient group. In all the subcortical regions examined in this study, the control group did not have any significant enhancements in functional connectivity when compared to the patient group.

3.1 Introduction

Social anxiety disorder (SAD), also known as social phobia, is characterized by a fear of negative evaluation and scrutiny by others (American Psychiatric Association, 2000) and is one of the most common psychiatric disorders with a lifetime prevalence rate of 6.8% (Kessler et al., 2005). However, despite its high occurrence rate and associated social and economic burden, the neurobiology of the disorder remains poorly understood. In recent years, there has been increased interest in elucidating the pathophysiology and neuronal mechanisms underlying SAD, particularly through the use of resting-state functional connectivity MRI (fcMRI) (Biswal et al., 1995). Of the existing fcMRI studies involving SAD populations, a few studies studies (Ding et al., 2011; Liao et al., 2010a; Liao et al., 2010b; Liao et al., 2011; Qiu et al., 2011) used identical acquisition parameters including low-resolution (3.75 x 3.75 x 5 mm) voxels. Of the remaining studies, one had very limited coil sensitivity to detect Blood Oxygenation Level Dependent (BOLD) signal (Pannekoek et al., 2012), and two had limited head coverage and/or low resolution (Hahn et al., 2011; Prater et al., 2013). Since physiological noise, a major confound in fcMRI, dominates at low-resolution (Triantafyllou et al., 2005), high-resolution imaging is desirable in this context. BOLD contrast-to-noise ratio (CNR) benefits directly from time-series Signal-to-Noise Ratio (tSNR) gains, and our previous work has demonstrated that the higher sensitivity offered by multichannel arrays such as 32-Channel (32Ch) coil, would translate to improved detection of resting state networks in healthy adults (Anteraper et al., 2013).

The amygdala, an area that has previously shown disorder specific hyperactivity in SAD populations (Phan et al., 2006), was the primary focus of seed-selection for most of the published resting-state fcMRI studies, whereas others investigated alterations in the Default Mode Network (DMN). Specific regions of thalamus and cerebellum although considered to be part of the DMN (Zhang and Raichle, 2010) are yet to be fully evaluated in the context of fcMRI evaluations in SAD. Of these subcortical regions, anterior nucleus of thalamus is considered to be one of the principal contributors to a well-accepted collection of pathways associated with emotion processing, the disruption of which could manifest as alterations in the DMN (Jones et al., 2011). Cerebellar role in emotion processing has been demonstrated recently using task-based fMRI in healthy participants (Baumann et al., 2012). None of the seed-based fcMRI studies published to-date in SAD populations has examined resting state networks with seeds in basal ganglia regions such as the striatum and globus pallidus. It may be important to use fcMRI to probe BOLD signal originating from these regions, especially considering that a recent functional MRI (fMRI) meta-analysis confirmed the link between the basal ganglia and emotion (Arsalidou et al., 2012) in healthy controls (HC) and highlighted the involvement of the striatum and globus pallidus in processing emotion. More recently, task-based fMRI studies have associated atypical striatal activation to anxiety (Perez-Edgar et al., 2013). Additionally, the globus pallidus has been linked to anxiety disorders based on lesion studies (Lauterbach et al., 1994) and emotional processing (Lorberbaum et al., 2004) based on reports from Positron Emission Tomography (PET). Furthermore, PET studies have reported cerebral blood flow (CBF) changes specific to the striatum during anticipatory anxiety to electrical shock (Hasler et al., 2007).

Based on the above, our hypothesis was that resting-state functional connectivity abnormalities are possible in the basal ganglia, thalamus, and cerebellum in SAD populations.

Detecting such alterations may be potentiated by technological improvements offered by parallel array coils (e.g., 32Ch head coil) which boost the tSNR in fMRI, especially in the high resolution domain (Triantafyllou et al., 2011). To this end, we explored resting state networks in a medication naïve SAD population when compared to HC in subcortical brain regions associated with emotional processing.

3.2 Methods

3.2.1 Subjects

Seventeen medication naïve SAD patients (24.7 ± 6.3 yrs, 8 males, all right-handed) and 17 age, gender and handedness matched healthy controls (25 ± 7.5 yrs) participated in the study. The mean Liebowitz Social Anxiety Scale (LSAS) (Liebowitz, 1987) score for the SAD group was 77.9 ± 14.1. Four patients had co-morbid depression and four had a co-morbid anxiety disorder. Written informed consent was obtained from all participants for an experimental protocol approved by the MIT institutional review board.

SAD patients were recruited from a local anxiety treatment center and through advertisements in the community. To be eligible, SAD patients needed to have a DSM-IV diagnosis of SAD, generalized subtype, and a total LSAS score of ≥ 60. Additionally, patients were excluded for the following reasons: current suicidal or homicidal ideation, history of (or current) psychosis, or current diagnosis of alcohol or substance dependence (excluding nicotine). None of the patients were receiving pharmacotherapy or psychotherapy at the time of the study. Healthy controls were recruited from the general community by advertisement and were screened for current and lifetime psychopathology using the Structured Clinical Interview for DSM-IV Axis I Disorders (SCID; First et al., 1996). To be eligible, they must have had no current or lifetime diagnosis of a psychiatric illness.

3.2.2 Data Acquisition

Data acquisition was performed on a Siemens 3T scanner, MAGNETOM Trio, a Tim System (Siemens AG, Healthcare Sector, Erlangen, Germany), using a commercially available radio frequency (RF) receive-only 32Ch brain array head coil (Siemens AG, Healthcare Sector, Erlangen, Germany). The body coil was used for RF transmission. Extra padding with foam cushions was used for head immobilization. During the task, all subjects were asked to relax in the scanner with their eyes open and fixate on a cross hair, displayed centrally on the screen.

Single-shot gradient echo Echo Planar Imaging (EPI) was used to acquire whole-head data, prescribed along anterior commissure – posterior commissure (AC-PC) plane with A>P phase encode direction. The scan duration was six minutes and 24 seconds (62 time points, 2 "dummy" scans). The scan parameters used for TR/TE/Flip Angle/Voxel size were 6000ms/30 ms/90°/2x2x2 mm^3. The TR was chosen to be 6 seconds in this study in order to do whole-brain coverage at high resolution of 2mm isotropic voxel size with 67 slices. Image reconstruction was carried out using the vendor provided Sum-of-Squares algorithm. In addition, high-resolution structural scan was acquired using 3D MP-RAGE (magnetization-prepared rapid-acquisition gradient-echo) sequence. The scan parameters used for TR/TE/TI/Flip Angle/Voxel size were 2530 ms/3.39 ms/1100 ms/7°/1.3x1x1.3 mm^3.

3.2.3 Data Analysis

SPM8 (Friston, 2007) was employed for pre-processing the resting state fMRI time-series and structural scans. The steps on EPI data included motion correction and slice-time correction, normalization with respect to the EPI template (sampling size was matched to the native (2-isotropic) resolution) provided by SPM, and 3mm Gaussian smoothing. Structural scan was

normalized with respect to SPM's T_1 template. Finally, image segmentation (Ashburner and Friston, 2005) was carried out on the T1-weighted images to yield grey matter (GM), white matter (WM) and CSF masks in normalized space.

3.2.3.1 First-Level Connectivity Analyses

Functional connectivity analysis was performed using MATLAB (MathWorks, Natick, MA) based custom software package: CONN (Whitfield-Gabrieli and Nieto Castanon, 2012). Sources for seed-based analysis were defined as multiple seeds corresponding to the pre-defined seed regions for: (*i*) striatum (caudate, and L and R putamen), (*ii*) globus pallidus (medial and lateral for internal and external segments respectively), (*iii*) thalamus, and (*iv*) L and R cerebellum. All seeds were independent of our data and were generated using WFU_PickAtlas (Maldjian et al., 2004; Maldjian et al., 2003). Seeds for thalamus (0, -12, 9) and cerebellum (±25, -81, -33) were chosen to be 10-mm spheres centered on previously published foci (Zhang and Raichle, 2010). Mid-brain sources (seeds) are depicted in Figure 3.1.

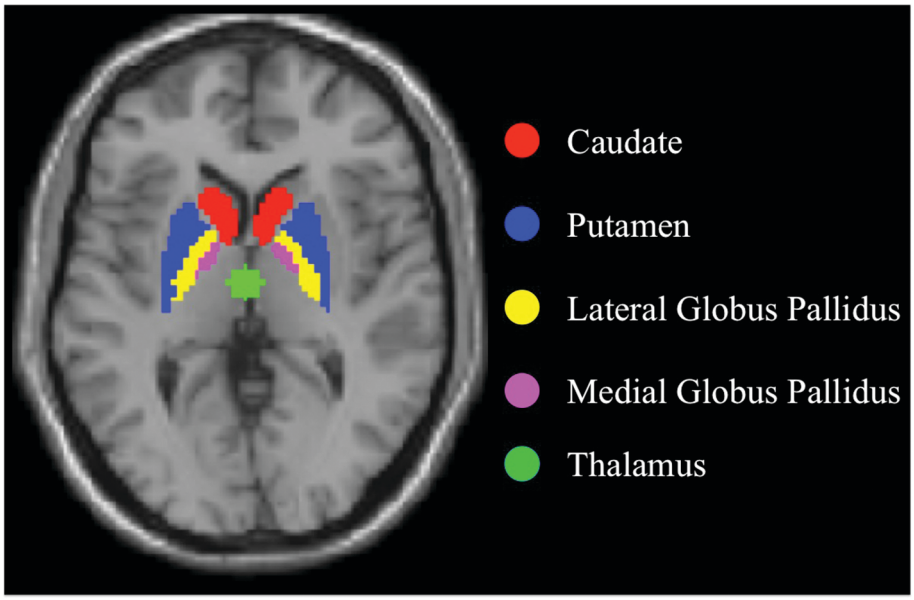

Figure 3.1: Mid-brain regions of interest that were chosen as sources to detect sub-cortical resting state networks.

Seed time-series were band-pass filtered (0.008 < f < 0.09 Hz) and non-neuronal contributions from WM and CSF were considered as noise, the principal components of which were estimated and removed using aCompcor (anatomical component based noise correction method) (Behzadi et al., 2007). The optimal configuration of the aCompCor approach as applied in the CONN toolbox was followed (Chai et al., 2011). In-house custom software (nitrc.org/projects/artifact_detect/) was used for detecting motion outliers, which were then included as nuisance regressors along with the seven realignment (3-translation, 3-rotation, 1-composite motion) parameters. At the scan-to-scan motion threshold used in this study (0.5mm translation and 0.5 degree rotation), there were 20 outliers in the SAD group and 13 in the HC group. There were no significant differences (p=0.45) in the number of outliers between the SAD and HC groups with mean values, 1.17±0.47 and 0.77±0.34 respectively.

Correlation maps were produced by extracting the residual BOLD time-course from the sources, followed by generating Pearson's correlation coefficients between the source time-course and the time-courses of all other voxels in the brain. Correlation coefficients were converted to normally distributed scores using Fisher's r-to-z transform in order to carry out second-level General Linear Model analyses. Images from the first-level results (correlation maps and z-maps) provided the seed-to-voxel connectivity maps for each selected source for each subject and for each condition (one per subject/condition/source combination).

3.2.3.2 Second-Level Connectivity Analyses

Within- and between-group analysis of data sets from the SAD and HC groups was performed as second-level analyses. For within-group comparisons, whole-brain False Discovery Rate (FDR) corrected threshold of p<0.05 ($p_{FDR\text{-}corr}$<0.05) was used to identify areas of significant functional connectivity. For between-group comparisons, statistical analysis was

performed using a cluster-defining voxel-wise height threshold of $p<0.05$ (uncorrected), and only the clusters with an extent threshold of whole-brain Family Wise Error (FWE)-corrected $p<0.05$ ($p_{FWE\text{-}corr}<0.05$) were reported as statistically significant.

3.3 Results

Within group results for the SAD and HC groups, with the caudate as the seed region, are shown in Figure 3.2 A. Positive correlations in the medial frontal gyrus (MFG), the dorsal anterior cingulate cortex (ACC) extending to the subgenual cortex and the orbito-frontal cortex (OFC) were significantly enhanced in the SAD group. Between group comparisons revealed hyper-connectivity (Figure 3.2 B), specifically in the MFG including the superior frontal gyrus (SFG) (BA 8), the dorso-lateral pre-frontal cortex (DLPFC) (BA 9), the middle frontal gyrus (BA 10), the orbital gyrus (BA 11), the subcallosal gyrus (BA 25), the ACC (BA 32), and the left temporal cortex (specifically, middle temporal gyrus (MTG) (BA 21) and inferior temporal gyrus (ITG) (BA 20).

Similarly, for the L and R putamen seeds (Figure 3.3 A), within group comparisons revealed hyper-connectivity in the fronto-parietal regions within the SAD group. In addition, connectivity with ITG and the parahippocampal gyrus (PHG) was absent within the control group (Figure 3.3 B). Connectivity was significantly enhanced in the SAD > HC comparison (Figure 3.3 C) in the bilateral supramarginal gyrus (BA 40), the rectal gyrus (BA 11), the pre-motor cortex (BA 6) and the ventral/subgenual ACC (BA 24/25), indicating interruptions in striatal function.

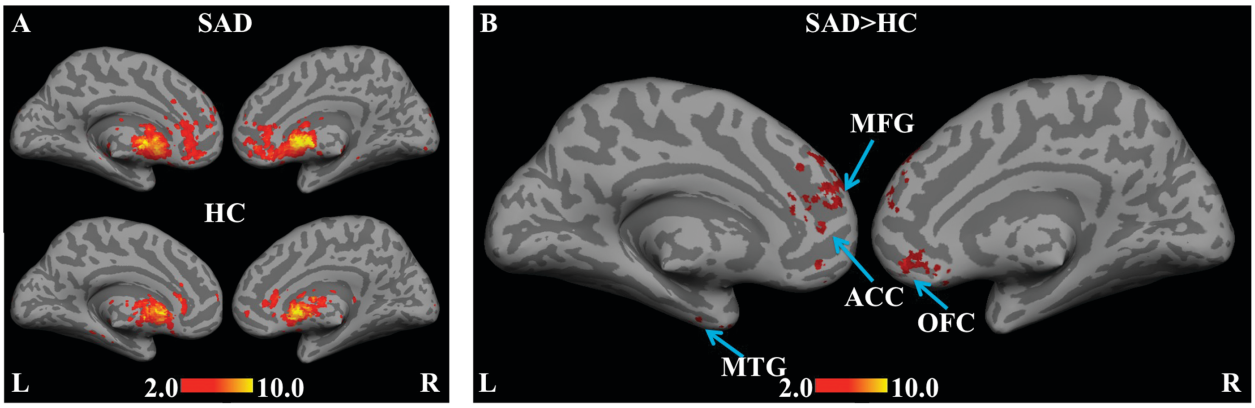

Figure 3.2: Statistical functional connectivity maps for caudate (second-level analysis, n=17 per group). Within-group height threshold is whole-brain $p_{FDR\text{-}corr}$<0.05 (Figure 3.2 A). SAD>HC reveals hyper-connectivity in medial frontal gyrus, ACC and left MTG (Figure 3.2 B, blue arrows). Between-group height threshold is p<0.05, cluster-level $p_{FWE\text{-}cor}$<0.05. HC>SAD contrast is not significant.

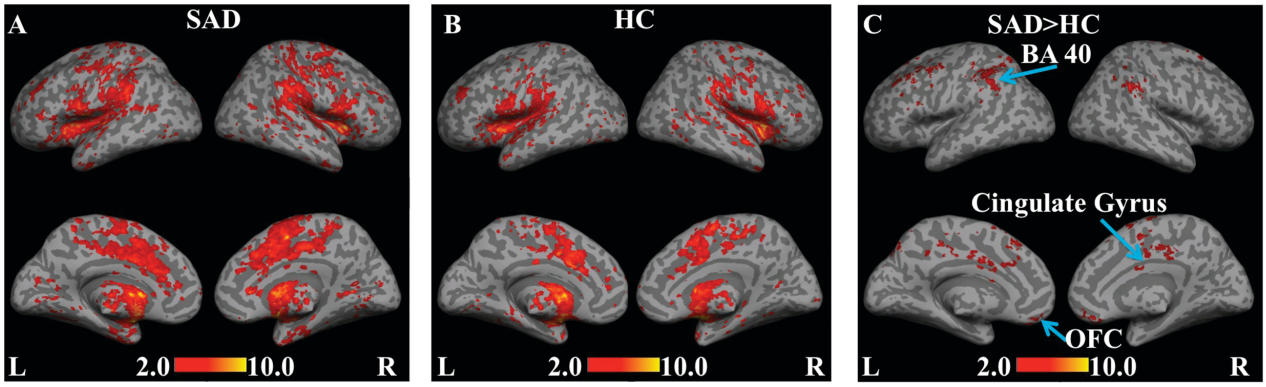

Figure 3.3: Statistical functional connectivity maps for putamen seeds (second-level analysis, n=17 per group). Within-group height threshold is whole-brain $p_{FDR\text{-}corr}$<0.05 (Figure 3.3 A, B). SAD>HC reveals hyper-connectivity in bilateral Supramarginal Gyrus, Rectal Gyrus, pre-motor cortex, and ventral/subgenual ACC (Figure 3.3 C, blue arrows). Between-group height threshold is p<0.05, cluster-level $p_{FWE\text{-}cor}$<0.05. HC>SAD contrast is not significant.

Furthermore, enhanced connectivity in the SAD group was revealed when the globus pallidus was used as a seed (Figure 3.4 A). In particular, the network consisting of the MFG, DLPFC, ACC and temporopolar area (BA 38) was more evident in the SAD group compared to the HC group. For the SAD > HC contrast (Figure 3.4 B), hyper-connectivity was observed in the precuneus (BA 31), signifying the possible role of mid-brain regions as contributors to the DMN.

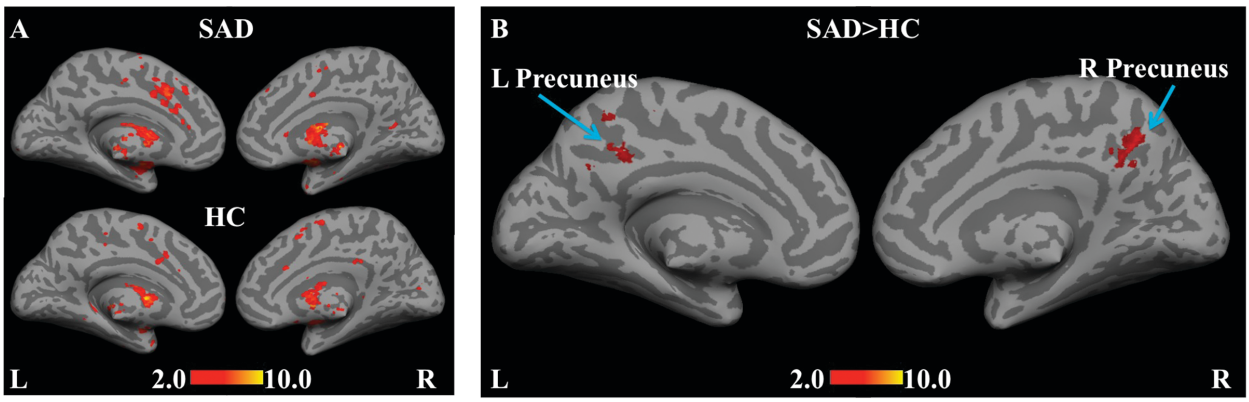

Figure 3.4: Statistical functional connectivity maps for internal and external segments of globus pallidus (second-level analysis, n=17 per group). Within-group height threshold is whole-brain $p_{FDR\text{-}corr}<0.05$ (Figure 3.4 A). SAD>HC reveals hyper-connectivity in Precuneus (Figure 3.4 B, blue arrows). Between-group height threshold is $p<0.05$, cluster-level $p_{FWE\text{-}cor}<0.05$. HC>SAD contrast is not significant.

Figure 3.5 A shows group-level results for the thalamus seed for the SAD and HC groups. Similar to the previous networks, positive correlations in the posterior cingulate cortex (PCC), and BAs 6, 7, 9, 10, 13, 24, 32 and 40 were stronger in the SAD group. Connectivity with primary, secondary and associative visual cortices (BAs 17, 18 and 19 respectively) were present only within the SAD group. Parts of the DMN such as the precuneus, bilateral ITG extending to the left and right PHG and parts of the fronto-parietal network involving superior parietal and anterior pre-frontal regions were significantly pronounced for the SAD > HC comparison (Figure 3.5 B). This finding emphasizes the role of the thalamo-cortical connectivity in SAD.

Figure 3.6 A shows the functional connectivity correlation maps generated at the second level for the L and R cerebellum seeds. Connections in medial pre-frontal cortices (MPFC), the PCC and BA 38 were stronger in the SAD group. Positive functional connectivity paralimbic regions such as entorhinal (BA 28) and perirhinal (BA 35) cortices were present only within the SAD group. Notably, the SAD > HC comparison revealed left lateralized hyper-connectivity in the amygdala (Figure 3.6 B).

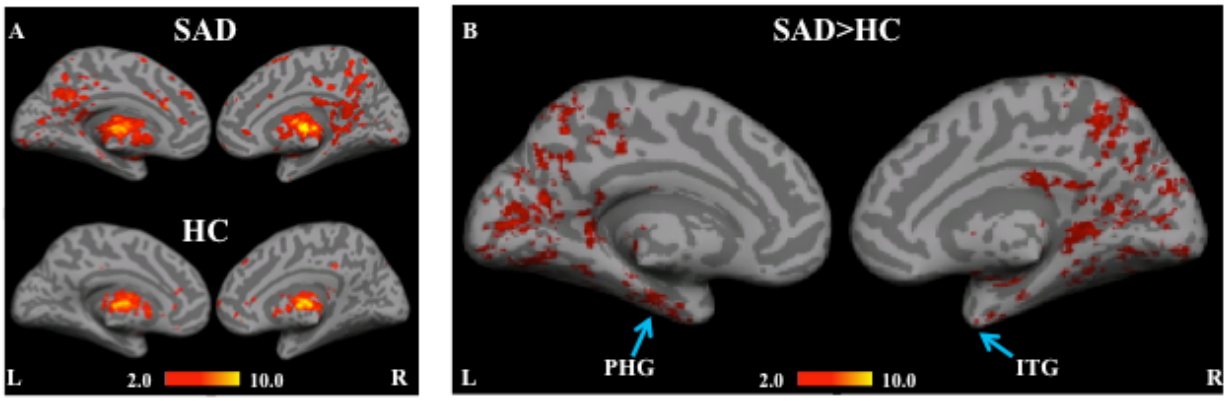

Figure 3.5: Statistical functional connectivity maps for thalamus seed (second-level analysis, n=17 per group). Within-group height threshold is whole-brain $p_{FDR\text{-}corr}$<0.05 (Figure 3.5 A). SAD>HC reveals hyper-connectivity in parahippocampal gyrus (PHG) and inferior temporal gyri (Figure 3.5 B, blue arrows). Between-group height threshold is p<0.05, cluster-level $p_{FWE\text{-}cor}$<0.05. HC>SAD contrast is not significant.

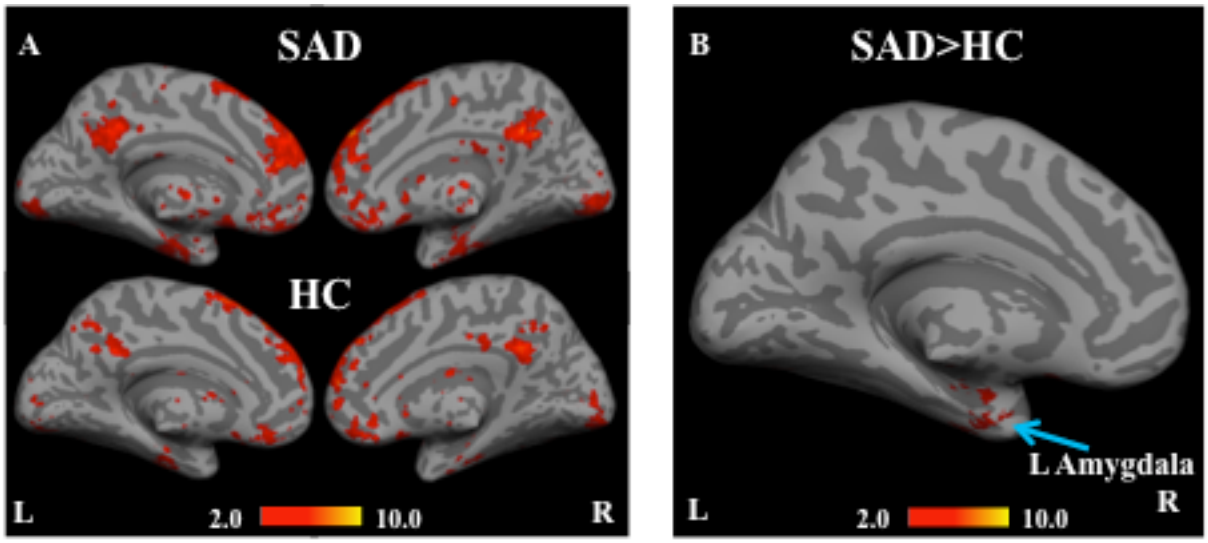

Figure 3.6: Statistical functional connectivity maps for cerebellum seeds (second-level analysis, n=17 per group). Within-group height threshold is whole-brain $p_{FDR\text{-}corr}$<0.05 (Figure 3.6 A). SAD>HC reveals hyper-connectivity in left amygdala (Figure 3.6 B, blue arrow). Between-group height threshold is p<0.05, cluster-level $p_{FWE\text{-}cor}$<0.05. HC>SAD contrast is not significant.

For all the regions/seeds explored in this study, the within group SAD contrast revealed stronger and more extensive connections within the basal ganglia and thalamus regions. In addition, we verified that the hyper-connectivity revealed in SAD>HC contrast was not driven by anticorrelations in controls. Notably, the HC > SAD contrast was not significant. Between-group results are summarized in Table 3.1.

Brain Region	Brodmann Area	Peak cluster	Voxels per cluster	T_{max}
Striatum/Caudate				
Medial Frontal Gyrus	BA 8/9/10/11	-2 44 -8	1576	5.35
ACC	BA 32	0 48 10		
Left Temporal Lobe	BA 38	-42 12 -32	772	4.37
Left Middle Temporal Gyrus (MTG)	BA 21	-54 -4 -26		
Striatum/Putamen				
right Supramarginal Gyrus	BA 40	48 -42 36	448	5.13
Rectal Gyrus	BA 11	6 38 -20	433	4.50
Premotor Cortex	BA 6	-26 20 60	2090	4.47
left Supramarginal Gyrus	BA 40	-48 -44 38	1189	4.43
ventral Anterior Cingulate Cortex (ACC)/Subgenual ACC	BA 24/25	-4 2 34	582	4.28
Globus Pallidus (medial and lateral)				
Precuneus	BA 31	8 -58 40	470	3.89
Thalamus				
Posterior Cingulate Cortex (PCC)	BA 30	-16 -40 4	5433	5.43
left Superior Temporal Gyrus (STG)	BA 22	-62 -60 14		
right Superior Parietal Cortex	BA 40	14 -70 64	1598	5.12
Precuneus	BA 31	8 -52 50		
left Parahippocampal Gyrus (PHG)	BA 36	-30 -16 -28	1520	4.88
left Inferior Temporal Gyrus (ITG)	BA 20	-60 -44 -16		
right PHG	BA 36	28 -16 -32	974	4.85
right MTG	BA 21	52 2 -34		
right PHG	BA 36	34 -4 -18	730	4.55
right Inferior Parietal Lobule	BA 40	38 -48 28		
right Inferior Frontal Gyrus (IFG)	BA 46	48 24 -8	1099	4.49
right STG	BA 22	48 -4 4		
Cerebellum				
left Amygdala	BA 34	-20 -10 -18	486	4.44

Table 3.1: Positively correlated brain regions for SAD > HC contrast (second-level analysis, n = 17 per group, cluster-level $p_{FWE\text{-}cor}<0.05$) for the sub-cortical regions explored in this study are given below. Opposite contrast was not significant.

3.4 Discussion

In this study, we explored subcortical resting state fcMRI in a SAD population. By probing the striatum (caudate and putamen), globus pallidus, thalamus and cerebellum, our study provides an important contribution to the literature and may prove useful for developing and improving treatment strategies. Unlike most of the published fcMRI studies on SAD, we employed a drug naïve sample in the current study because of the known influence of pharmacotherapy (Warwick et al., 2012).

Although there is little debate on the role of subcortical regions in the pathophysiology of SAD, functional connectivity alterations with these regions as seeds have remained either unexplored or inconclusive in previously published resting-state fcMRI studies. Analyses of the caudate seed in the current study revealed significantly higher functional connectivity between temporal and frontal regions such as the orbital, medial, inferior and anterior cingulate cortex in the SAD > HC comparison. This could be indicative of abnormalities in frontal-subcortical circuits associated with SAD, as previously shown when using a frontal medial seed in exploring task-based functional connectivity (Gimenez et al., 2012). Moreover, task-based hyperactivity in frontolimbic regions has been previously reported in the context of SAD (Veit et al., 2002), which could be indicative of the abnormalities associated with the underlying pathology. Alterations in the fronto-parietal regions were also observed with L and R putamen seeds in the current study. These findings could help explain some of the deficits in the Executive Control Network in the resting-state (Seeley et al., 2007) in SAD populations as previously observed (Liao et al., 2010a). Our study also revealed hyper-connectivity in the ventral/subcallosal ACC with the putamen seeds. Hyperactivity in this region has been attributed to social anxiety from task-based fMRI studies (Ball et al., 2012). The subcallosal ACC has also been classified as part of the "Affective Network" in previous studies (Sheline et al., 2010). Taken together, the hyper-connectivity of cingulate gyrus with the caudate and putamen seeds, as demonstrated in this work, could be indicative of disturbances in striatal function specific to SAD. This is consistent with previous reports from nuclear imaging (van der Wee et al., 2008). Enhanced connectivity in pre-motor regions suggests that SAD patients are in a state of "motor readiness", either due to abnormal input to the striatum (from amygdala or mid-brain dopaminergic neurons) as proposed as a testable model for anxiety disorders by (Marchand, 2010). Enhanced functional connectivity

with striatum and regions of the OFC with SAD is equally interesting because of recent reports from task-based fMRI, highlighting the role of OFC in neural habituation in SAD (Sladky et al., 2012).

Smaller structures such as the globus pallidus are typically excluded from fcMRI evaluations of mid-brain regions because of inadequate coil sensitivity and low-resolution acquisition (Di Martino et al., 2008). Our decision to include the globus pallidus in this study stems from our previous fcMRI study demonstrating the benefits of using multichannel arrays in the high-resolution regime for investigating mid-brain regions (Anteraper et al., 2013). The globus pallidus has been classified in a recent meta-analysis (Hattingh et al., 2012) as one of the regions (along with amygdala, entorhinal cortex, ITG, ACC and post-central gyrus) that is significant in the SAD > HC comparison for task-based fMRI involving emotional stimuli. We found hyper-connectivity of the globus pallidus and the precuneus for the first time in the SAD domain with seed-based resting state fcMRI. Interestingly, previous studies have reported connectivity between these two regions with effective connectivity measures (Marchand et al., 2007). PET studies involving deep brain stimulation of the globus pallidus in Huntington Disease have reported decreased regional CBF in the precuneus (Ligot et al., 2011). Precuneus is considered to be part of the self-referential network, the alterations of which have been previously explored in the realm of task-based fMRI in SAD, particularly for the evaluation of mindfulness-based intervention programs in unmedicated patients (Goldin et al., 2012).

Increased activity of the thalamus is one of the most consistent findings in neuroimaging studies of SAD populations (Freitas-Ferrari et al., 2010). Gimenez and colleagues (2012) have reported enhanced functional connectivity between thalamus and ACC in the SAD group, but had tSNR limitations (1.5T and 8Ch coil) and did not use a formal resting state paradigm (“rest”

blocks were combined from fMRI block design). In addition to ACC, our study revealed stronger positive correlations with the thalamus seed and pre-motor, frontal, dorsolateral pre-frontal, insular, and parietal cortices within SAD group. Significant enhancements in functional connectivity in the SAD > HC contrast was also noted for several thalamo-cortical regions including the precuneus, ITG and PHG, which are part of the DMN. Increased cortical thickness in the ITG has been associated with SAD in recent reports based on structural MRI studies (e.g., (Frick et al., 2013)). Additionally, significantly enhanced thalamo-cortical connections, specifically in the anterior pre-frontal and superior parietal cortices, supports the existence of a fronto-parietal network that compensates for the deficits associated with anxiety disorders, as previously illustrated by (Etkin et al., 2009). Finally, hyper-connectivity of the bilateral PHG in SAD is particularly noteworthy because PHG has been reported as a major hub in the medial temporal lobe, in association with the DMN (Ward et al., 2013).

Significantly stronger temporal correlations between the cerebellar seeds and the amygdala in the SAD group (which was not present in HC > SAD contrast) underscore the relevance of the cerebellum in emotion processing. Parallels have been drawn from animal studies between the amygdala and cerebellum dependent conditioning of fear (Medina et al., 2002) emphasizing the involvement of cerebellum in emotion. Liao and colleagues (2010b) have previously reported abnormal effective connectivity with cerebellum in the context of SAD when bilateral amygdalae were chosen as seeds for Granger causality analysis. Resting state fcMRI in healthy populations has also provided converging evidence for the functional connectivity of the amygdala and cerebellum (Sang et al., 2012). In addition, cerebellar involvement in the SAD group for a "scrutiny network" (comprised of regions in medial frontal cortex, bilateral insula and the cerebellum) has also been revealed by fMRI using a perception of scrutiny task

(Gimenez et al., 2012). The left lateralization of amygdalar hyper-connectivity is an encouraging finding because hyperactivity in the left amygdala has been reported previously in the context of depression (with task-based fMRI), which subsequently normalized with antidepressant treatment (Sheline et al., 2001). The left lateralization that we observed in this study is also consistent with previous meta analyses on emotional processing studies involving fMRI and PET, highlighting hyperactivity in the left amygdala compared to the right (Baas et al., 2004). Hahn and colleagues (2011) have also reported hyperactivity of left amygdala in the SAD group. Recent fMRI study on healthy adults has indicated left lateralized amygdala activity, specifically for processing negative stimulus (Beraha et al., 2012). More recently, structural MRI studies have shown increases in gray matter in the left cerebellum in SAD patients (Talati et al., 2013).

Our results highlight the synergy of utilizing multichannel array coils and high resolution in deciphering the resting-state BOLD fluctuations, particularly from sub-cortical regions such as basal ganglia and cerebellum in the context of SAD.

Chapter 4

Optimization of Simultaneous Multi-Slice Acquisition for Resting State Functional Connectivity MRI

Abstract

Application of simultaneous multi-slice (SMS) acquisition in functional Magnetic Resonance Imaging (fMRI) experiments employing single-shot Echo Planar Imaging (EPI) protocols provides improved temporal resolution (short repetition times (TR)). This is particularly important in functional connectivity MRI (fcMRI) for removing non-neuronal contributions such as fluctuations in physiological noise (cardiac, respiratory and CSF pulsations). Increasing spatial resolution is one way to reduce physiological noise because multichannel arrays can compensate the SNR hit from reduced voxel volumes. However, this results in EPI protocols with high TRs, which brings about a different set of issues such as aliasing of cardiac and respiratory signals into the frequencies of interest (<0.1 Hz) in resting-state fcMRI. In this study, by employing SMS-EPI as the workhorse, we compare signal detectability with 32-Channel (32Ch) array coil in a series of temporal resolutions with SMS factors ranging from 3 through 7 using seed-based connectivity analyses. The primary aim was to optimize the acquisition parameters in the context of SMS using a recently available work-in-progress sequence from Siemens and to investigate whether the higher SMS factors can extract and map spontaneous activity fluctuations in an efficient manner by merit of higher temporal resolution. Functional connectivity mapping was chosen for the purpose of comparison because the spatial coherence of these networks is well understood and is robust and reliable across

healthy subjects. Whole-brain comparisons revealed that higher SMS factors (i.e., high temporal resolutions) provided increased detailed functional connectivity in the default mode network (DMN). In addition, comparisons between the 32Ch and 12-Channel (12Ch) array coils at higher SMS factors such as 7 (TR=800 ms) also revealed detailed functional connectivity maps, even from subcortical regions such as thalamus, as part of the DMN. Switching to higher temporal resolutions and multichannel arrays like 32Ch coil may be beneficial for fcMRI studies. Finally, SMS acquisition with and without in-plane acceleration was carried out to investigate whether resting state networks from susceptibility prone areas could be restored by merit of the geometric distortion mitigation of parallel imaging.

4.1 Introduction

Of all the resting state networks identified so far, the default mode network (DMN), consistent with reports from metabolic imaging studies (Raichle et al., 2001), has received the most attention in the clinical and research community (Buckner et al., 2008; Fransson, 2006; Greicius et al., 2003). Furthermore, it has been identified as one of the strongest hubs of all the brain networks in the resting state (Tomasi and Volkow, 2011).

One of the trade-offs that has to be made for attaining whole-brain coverage, which is important for detecting anatomically distant spontaneous low frequency temporal correlations in resting state fcMRI studies, is between repetition time (TR) and spatial resolution. Advantages of moving towards high spatial resolution (small voxel volumes) include reductions in signal drop out via through plane de-phasing (because of thinner slices) and lesser contamination by partial volume effects (better localization of BOLD). Since time-series signal-to-noise ratio (tSNR) is directly proportional to BOLD contrast-to-noise ratio, one of the most important metrics in fMRI, higher sensitivity offered by multichannel arrays (e.g., 32 Ch coil) especially at higher

resolutions, could translate directly to improved detection capabilities for accurately identifying resting state functional connectivity networks (Anteraper et al., 2013). However, to achieve higher spatial resolution such as 2x2x2 mm^3 without employing parallel imaging, TR has to be about 6 seconds, which is not the best-case scenario because of contamination with physiological noise such as heart rate and respiration. This is not necessarily the case if one could bring the technologies of high field strength (3-Tesla or more) and multichannel array coils together with parallel imaging strategies such as GRAPPA (Generalized Autocalibrating Partially Parallel Acquisition), not just in the phase dimension but also in the slice dimension by using simultaneous multi-slice (SMS) acquisitions (Feinberg et al., 2010; Setsompop et al., 2012). In-plane acceleration provided by GRAPPA as originally described (Griswold et al., 2002) is by the merit of the spatial encoding provided by array coils. As the number of array coils increases, provided the coil geometry is optimized for the region being imaged, there can be remarkable improvements in scan time reductions as demonstrated recently (Keil et al., 2012).

Higher temporal resolutions offered by SMS sequences remain yet to be systematically explored in fcMRI. The primary goal of this work is to explore whether the higher sensitivity of a 32Ch array coil when used with SMS sequence, would translate directly into improved detection capabilities for accurately identifying the DMN. Resting state fcMRI from DMN will be evaluated in the high-resolution EPI regime for this purpose using seed-based connectivity analyses. In addition, we investigate whether slice acceleration/GRAPPA with SMS-EPI, in combination with in-plane GRAPPA can prove beneficial in ameliorating susceptibility-artifacts so as to improve the detection of resting state fcMRI networks. For this, seed-based analysis will be performed from Orbito-Frontal Cortex (OFC), a region that suffers from severe geometric distortion due to its location and slow EPI phase encoding.

4.1.1 Theory

The radio frequency (RF) pulse as a function of time t, implemented in SMS imaging is described by equation 4.1 below.

$$RF(t) = sinc(t)e^{i\omega t} \quad (4.1)$$

The SMS protocols evaluated in this study is a work-in-progress sequence made available by Siemens based on the blipped-CAIPI (Controlled Aliasing in Parallel Imaging) implementation of Setsompop and colleagues (Setsompop et al., 2012). Provided below is a brief overview of the slice GRAPPA technique as described in (Setsompop et al., 2012). The main difference between this technique and in-plane GRAPPA is that instead of using the existing coil sensitivity on k-space data to retrieve information on lines to be filled in, slice GRAPPA calibration fills in k-space information per coil per slice based on equation 4.2 given below:

$$C_{j,z}(x,y)\rho_z(x,y) = \sum_{l=1}^{L} C_{l,collapse}\,(x,y)\rho_{collapse}(x,y)K_{l,j,z(x,y)} \quad (4.2)$$

$C_{j,z}(x,y)$, $\rho_z(x,y)$, $\rho_{collapse}(x,y)$, $and\ K_{l,j,z(x,y)}$ denote sensitivity profile from jth coil, image of slice z, collapsed image and GRAPPA kernels respectively. However, as explained in (Setsompop et al., 2012), the image dependency of equation 2 vanishes and it reduces to equation 4.3 below under typical imaging (because of the field-of-view shift imparted in the slice dimension by "blipped-CAIPI" pulses), thereby making GRAPPA kernels to be dependent solely on coil sensitivity (as in the case of in-plane GRAPPA).

$$C_{j,z}(x,y) = \sum_{l=1}^{L} C_{l,z}\,(x,y)K_{l,j,z(x,y)} \quad (4.3)$$

4.2 Methods

4.2.1 Power Analysis

Regardless of analysis techniques and acquisition protocols, "power failure" is a big issue in any study reporting statistical comparisons (Button et al., 2013). In this study, fmripower (fmripower.org) was used for power analysis for detecting statistically significant temporal correlations utilizing the steps reported in a previous study (Mumford and Nichols, 2008). A resting state data set from the 12Ch coil (independent from the current study) was used for the purpose. N of 6 was shown to retain sufficient power (defined as 1-β, where β refers to the rate of rendering type II error) to detect functional connectivity using PCC as seed (see Figure 4.1 below).

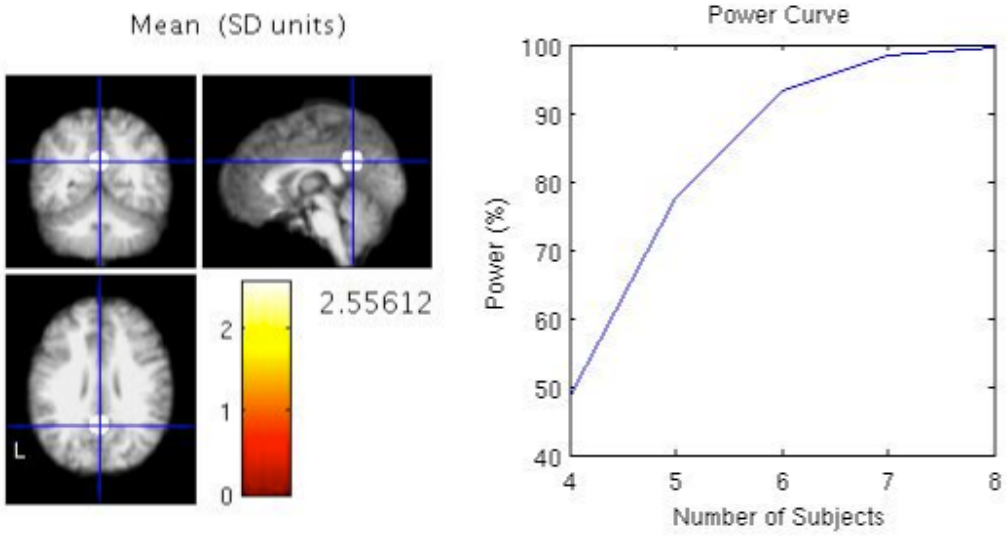

Figure 4.1: Power analysis plots indicate that N of 6 is sufficient to have more than 80% power with PCC as seed ROI with a p-threshold of 0.005 (for type I error).

4.2.2 Subjects

For preliminary evaluation of the SMS protocols (which is a work in progress), we enrolled 6 healthy volunteers (3 men), all right-handed, with mean age 24 (age range 18-28). Written informed consent was obtained for the experimental protocol approved by the

institutional review board. To minimize head movement, extra care was taken when the participant was placed in the scanner; extra padding with foam cushions was used for head immobilization inside the head coils. During resting-state time-series acquisition, subjects were asked to relax with their eyes closed, and were instructed not to fall asleep. Automatic slice prescription, based on alignment of localizer scans to a multi-subject atlas (van der Kouwe et al., 2005), was used to achieve a consistent slice prescription.

4.2.3 Data Acquisition

Data acquisition was performed on a Siemens 3T scanner, MAGNETOM Trio, a Tim System, (Siemens AG, Healthcare Sector, Erlangen, Germany), using a 32Ch and 12Ch brain array product coils (Siemens Healthcare, Erlangen, Germany). For fcMRI acquisition, full head coverage was achieved with 2mm thick interleaved slices with orientation parallel to the AC-PC plane, in-plane spatial resolution of 2 mm x 2 mm. Each resting scan run lasted for ~5 minutes and all subjects were scanned with both head coils and SMS factors 3 through 7 (see Table 4.1 below for acquisition parameters). The flip angle was set to Ernst angle, with the T_1 of grey matter set to 1400 ms. Additionally, a 3D high-resolution T_1-weighted structural scan was acquired using a magnetization-prepared rapid-acquisition gradient-echo (MP-RAGE) sequence with voxel size = 1.3x1x1.3 mm^3, other acquisition parameters were: TR/TE/TI/FA=2530 ms/3.39 ms/1100 ms/7°.

4.2.4 Data Analysis

4.2.4.1 Artifact Detection and Rejection

Seven (3-translation, 3-rotation and 1-composite motion) parameters along with the motion outliers were used as nuisance regressors along with white matter and CSF segments

obtained from the segmentation routine implemented in SPM8 (Ashburner and Friston, 2005). In-house custom software (nitrc.org/projects/artifact_detect/) was used for detecting outliers. There were no significant differences (p-value=0.5) in the mean number of outliers between the 12Ch (13.83±5.6) and 32Ch (19.67±16.4) group for the group level comparisons carried out for SMS factor of 7 for quality control thresholds (scan-to-scan motion threshold of 0.4mm/0.4 degree and global signal threshold of 3 standard deviations from mean) used in this study.

4.2.4.2 First-Level Connectivity Analyses

Prior to connectivity analysis, data were realigned, normalized with respect to EPI template, and spatially smoothed using routines implemented in SPM8 (Friston, 2007a). Functional connectivity analysis was performed using a seed-based approach with MATLAB (MathWorks, Natick, MA) based custom software package: CONN (http://www.nitrc.org/projects/conn/). Seeds for DMN was chosen to be 10 mm spheres centered on previously published foci (Zhang and Raichle, 2010) for the Posterior Cingulate Cortex (PCC), medial pre-frontal cortex (MPFC) and left and right lateral parietal cortices (LLP and RLP) using WFU_PickAtlas (Maldjian et al., 2003). OFC seed was also defined in a similar manner around (0, 40, -25). Time-series extracted from the seed were temporally band-pass filtered ($0.008 < f < 0.09$ Hz). The optimal configuration of the anatomical Compcor (aCompCor) approach (Behzadi et al., 2007) as applied in the CONN toolbox was followed. Correlation maps were generated by extracting the residual BOLD time-course from the seeds of interest, followed by computing Pearson's correlation coefficients (r-values) between the seed time-course and the time-courses of all other voxels in the brain. Finally, correlation coefficients were converted to normally distributed scores using Fisher's r-to-z transform to allow for General Linear Model based second-level analyses.

SMS Factor	TR (ms)	Flip Angle (degrees)	Number of Slices	Number of Time Points
3	1410	72	51	215
4	1200	65	52	250
5	1000	61	55	300
6	800	56	54	376
7	800	56	63	376

Table 4.1: Data acquisition parameters for the SMS factors employed in this study with the corresponding repetition times, flip angles and number of slices and time points. All protocols employed whole-brain coverage, 2mm-isotropic resolution and partial-fourier encoding (6/8) of k-space.

4.2.4.3 Second-Level Connectivity Analyses

Within-group analysis of data sets from the 32Ch for SMS factors 3 through 7 was performed as second-level analyses. Only the voxels that surpassed a whole-brain False Discovery Rate (FDR) corrected threshold of $p<0.05$ were identified as areas of significant functional connectivity. For between-group comparisons between 32Ch and 12Ch head coils, statistical analysis was performed using a cluster-defining voxel-wise height threshold of $p<0.005$ (uncorrected), and only the significant clusters with an extent threshold of whole-brain Family Wise Error (FWE)-corrected $p<0.05$ were retained.

4.3 Results

Figure 4.2 shows the result of first level connectivity analysis from a representative subject for a conventional TR of 2 s and a fast TR of 800 ms. In all the four seeds (PCC, MPFC, LLP and RLP) of the DMN that were chosen for comparison, detailed functional connectivity is revealed with improvement in temporal resolution. TR shortening also allows more number of time-points to be packed in the same run that balances the potential tSNR drop that occurs with SMS imaging.

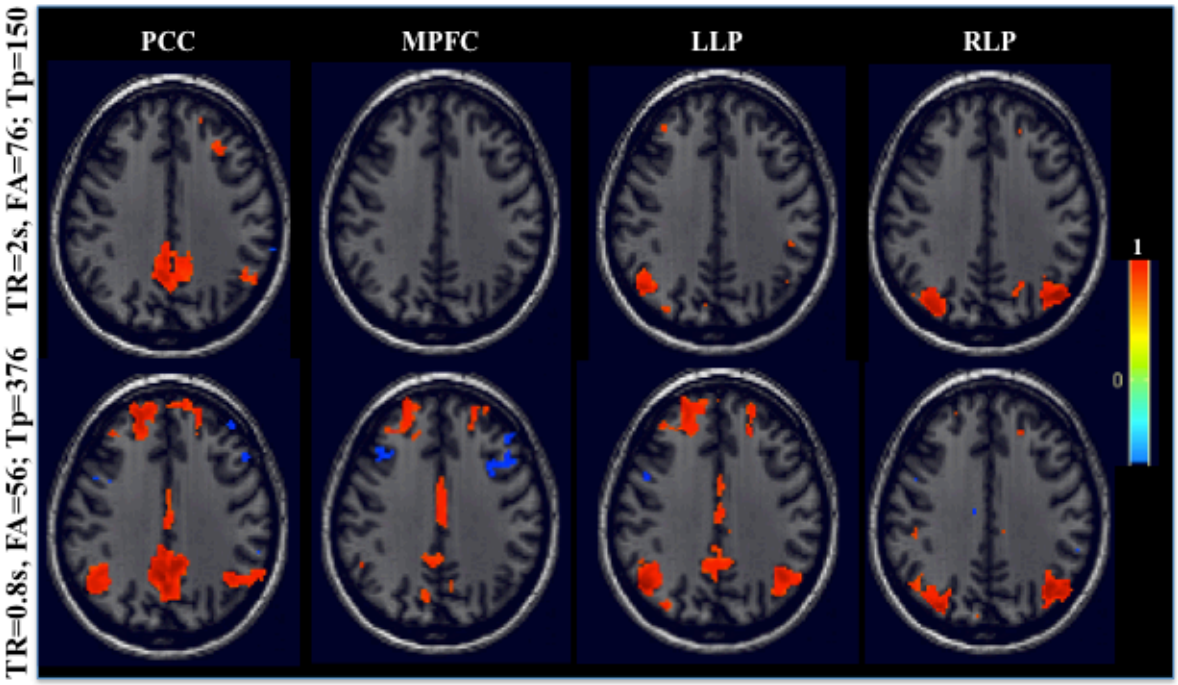

Figure 4.2: First level functional connectivity results from a representative subject with 4 different seeds corresponding to the DMN during 5 minute scan sessions. Correlation (r-value) threshold=0.6.FA=Flip Angle, T_p=Number of time points.

Figure 4.3 shows positive correlations detected from second level connectivity analysis using PCC as seed for a range of SMS factors. At the threshold used for comparison (whole-brain $p_{FDR\text{-}corr}<0.05$), only two voxels from the PCC (results not shown) were found to be significant for SMS factor of 3 (TR=1410 ms). The entire network consisting of MPFC, LLP and RLP of DMN (see white arrows, Figure 4.3) was revealed only with a TR of 800 ms, corresponding to SMS factor of 7. High N-array coils (e.g., 32Ch coil) are a requirement for retaining sufficient SNR. This is clear from the raw data shown in Figure 4.4 for SMS factor of 7 and as further demonstrated from the tSNR comparison of the central slice (Figure 4.5) and the functional connectivity maps for the 32Ch>12Ch contrast (Figure 4.6). Significant brain regions depicted by yellow arrows in Figure 4.6 are summarized in Table 4.2. Finally, the advantage of in-plane GRAPPA in combination with slice GRAPPA (with acceleration factors of 2 and 4 respectively) is shown in Figure 4.7.

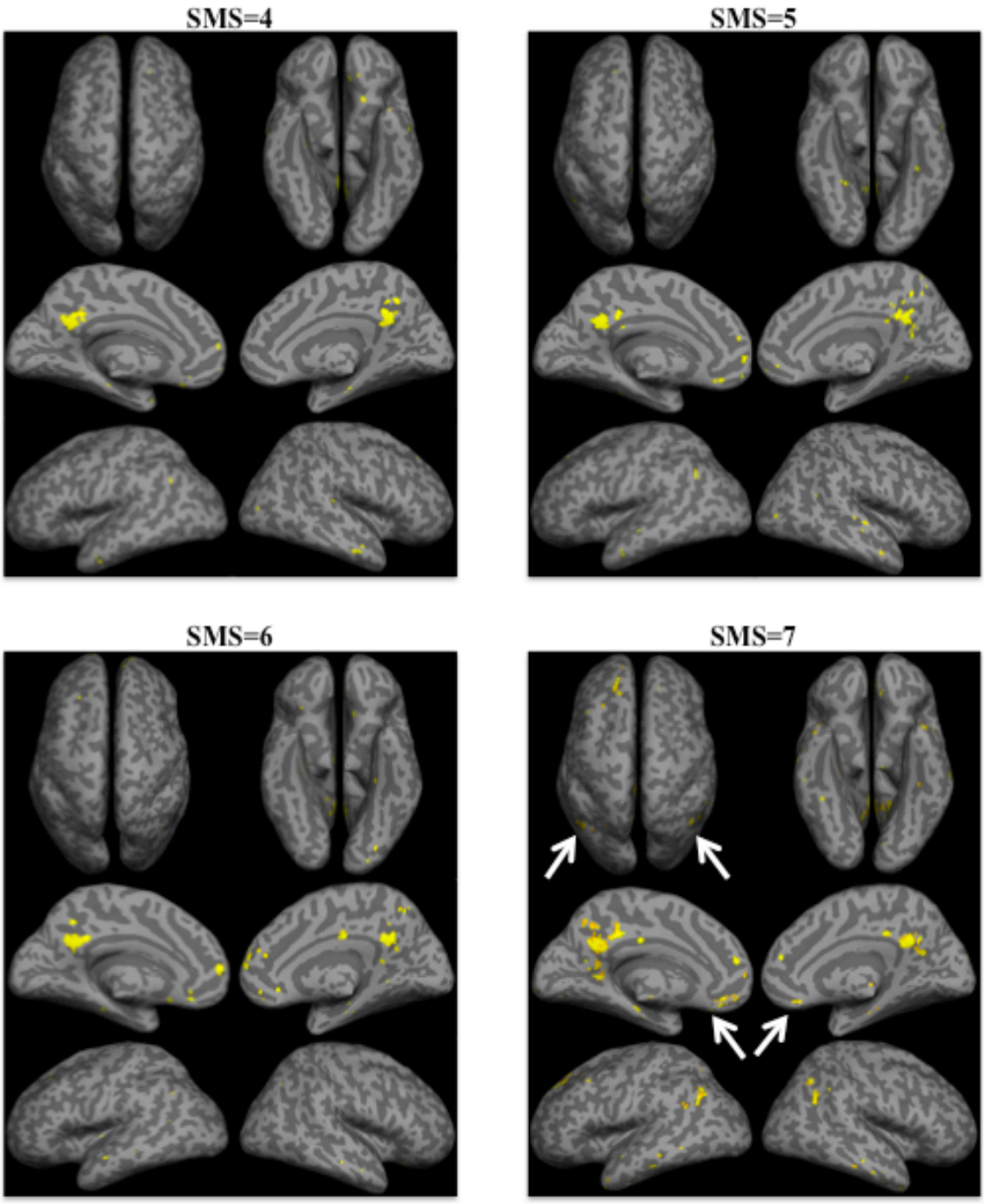

Figure 4.3: Statistical functional connectivity maps for seed region of interest from posterior cingulate cortex for four different slice accelerations (second-level analysis, N=6). Height threshold is whole-brain $p_{FDR\text{-}corr}$<0.05. The default mode network with left and right lateral parietal cortices, and medial pre-frontal cortices (white arrows) are revealed better with SMS factor of 7 (TR=800 ms).

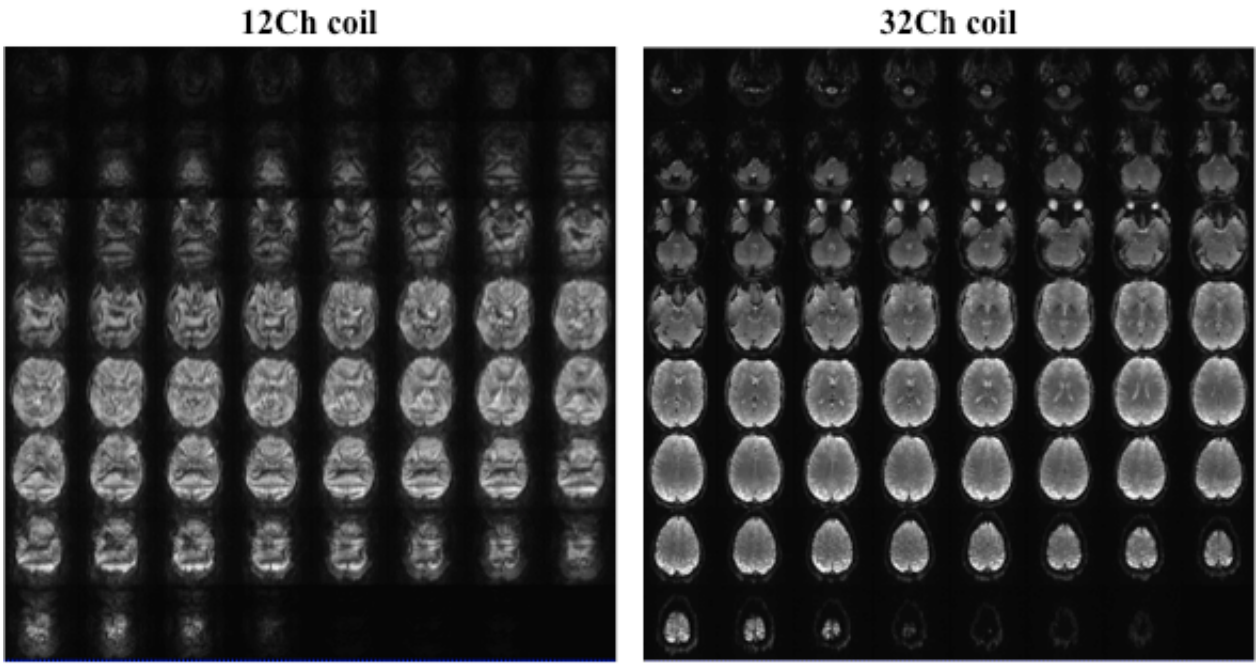

Figure 4.4: Comparison of data quality from 12Ch and 32Ch coils with SMS factor of 7 (TR=800 ms).

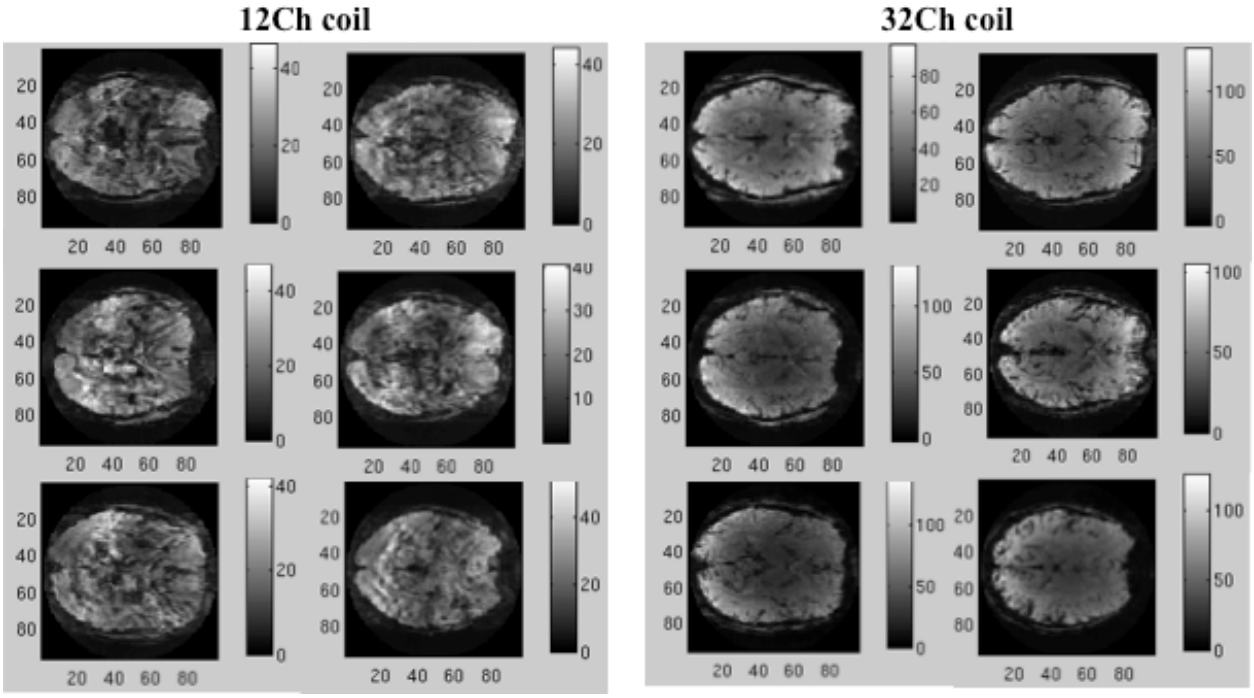

Figure 4.5: tSNR maps (mean divided by the standard-deviation computed on a pixel-by-pixel basis) for the central slice for SMS factor of 7 (TR=800 ms). Poor tSNR maps from 12Ch coil directly translated to poor BOLD contrast as demonstrated in Figure 4.6.

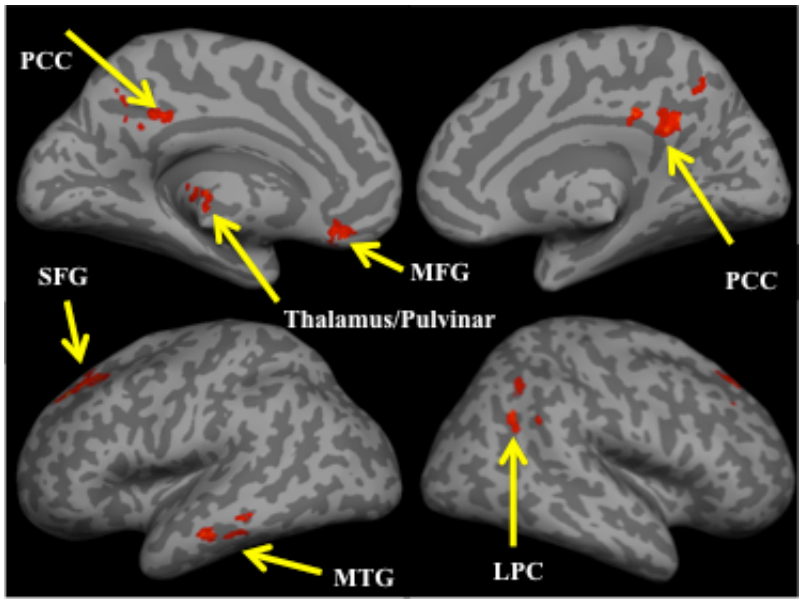

Figure 4.6: Statistical functional connectivity maps for the 32Ch versus 12Ch comparison from Posterior Cingulate Cortex (PCC) seed at MB =7 (second-level analysis, n=6 per group). 32Ch>12Ch contrast reveals significant positive correlations from the default mode network (height threshold is p<0.005, cluster-level $p_{FWE\text{-}cor}$<0.05). Opposite contrast is not significant. MFG=Medial Frontal Gyrus; MTG=Middle Temporal Gyrus; LPC=Lateral Parietal Cortex; SFG=Superior Frontal Gyrus.

Brain Region	Peak cluster	Voxels per cluster	T_{max}
Default Mode Network			
left Superior Frontal Gyrus	-22 42 40	169	9.85
Posterior Cingulate Cortex	-2 -38 36	269	7.30
Thalamus/Pulvinar	-12 -30 8	98	7.12
right Superior Frontal Gyrus	28 34 52	79	7.03
right Lateral Parietal Cortex	46 -56 32	101	6.98
Medial Frontal Gyrus	-2 36 -16	69	6.55
left Middle Temporal Gyrus	-60 -18 -16	81	6.26

Table 4.2: Positively correlated brain regions for the 32Ch>12Ch contrast (second-level group analysis, n = 6 per group; cluster-level $p_{FWE\text{-}cor}$<0.05; height threshold: T = 3.17) with posterior cingulate cortex as seed region of interest at SMS=7. Opposite contrast was not significant highlighting the merit of the 32Ch coil at higher temporal resolutions.

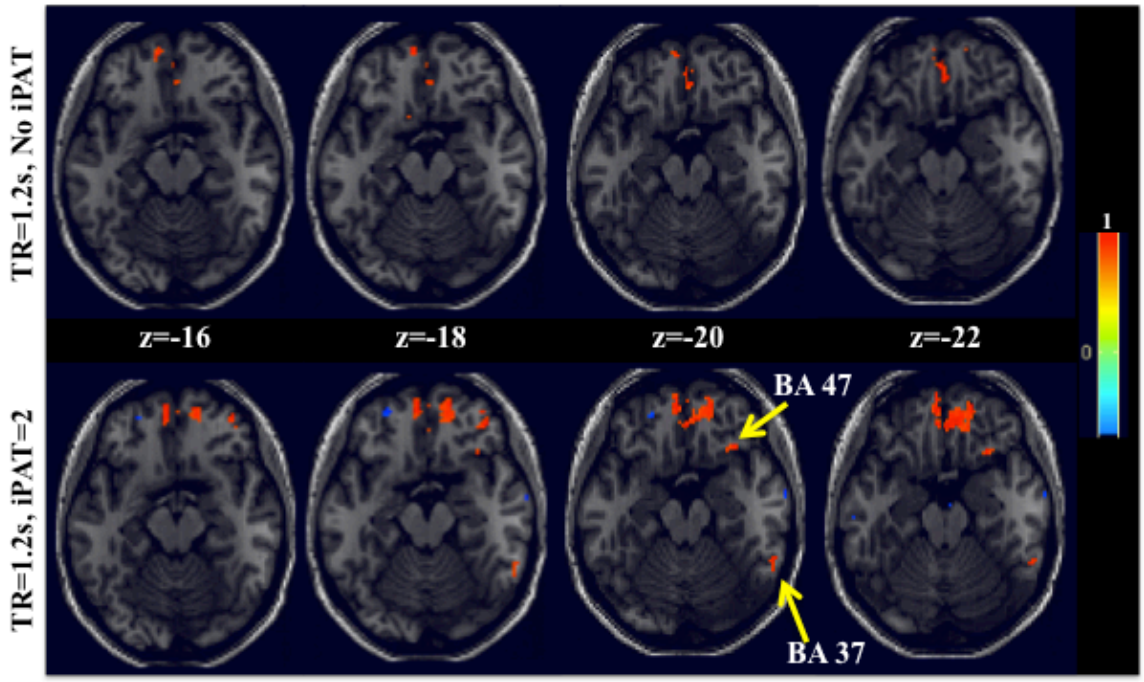

Figure 4.7: First level functional connectivity results from a representative subject with OFC seed, without (top row) and with in-plane acceleration of 2 (bottom row) from 4 consecutive slices in combination with SMS factor of 4 with 32Ch coil from a 5 minute scan session. Correlation (r-value) threshold=0.6. Positive correlations with inferior pre-frontal and inferior temporal cortices (Brodmann Area (BA) 47 and 37 respectively) are revealed only with in-plane acceleration demonstrating the usefulness of in-plane GRAPPA in detecting temporal correlations from regions that are prone to susceptibility artifacts. iPAT=integrated Parallel Acquisition Technique.

4.4 Discussion

Optimizing data collection parameters is critical to providing the best possible tSNR and spatial resolution from the available scanner hardware because acquisition parameters such as SMS factors could play significant impact on the data quality outcome. Longitudinal magnetization from grey matter is fully relaxed in less than 1.5 s. Therefore all the evaluations for the group comparisons are based on TR of 1.5 s or below. Based on our comparisons with PCC as seed, we have demonstrated that the use of imaging strategies such as SMS, in combination with multichannel array coils would offer significant reductions in TR/improvements in the temporal resolution that would elucidate resting state networks in a

detailed and significant manner at both subject and group level comparisons. This could also potentially ameliorate the effects of movement that is detrimental to tSNR (Van Dijk et al., 2010). The session length was chosen to be 5 minutes for detecting DMN, based on recommendations from an earlier study investigating the acquisition parameters for resting state fcMRI (Van Dijk et al., 2010). This could be increased to 10 minutes or more if the areas of interest involve sub-cortical regions such as amygdala and ventral tegmental areas that are prone to susceptibility artifacts. Mid-brain regions could also benefit from additional scan time or improved number of time points made available (without increasing the length of scan session) because of increased temporal resolutions. This is because recent studies have shown that even at 7T, the tSNR from mid-brain regions are poor as they are predisposed to CSF pulsations (because of their location), blood vessels and white matter tracts (Barry et al., 2013).

As expected from the comparisons outlined in Chapter 2, the 12Ch coil was not favorable for SMS acquisitions at high temporal resolutions such as TR=800 ms, because of the limitations in coil sensitivity. Between-group comparisons revealed statistically significant differences in the 32Ch>12Ch contrast for all the key nodes of the DMN such as PCC, MPFC and left and right LPC (Fox et al., 2005) for SMS of 7 highlighting the limitation of 12Ch coil at high temporal resolutions. In plane acceleration of 2 in combination with SMS factor of 4 provided detailed functional connectivity from OFC seed, highlighting the advantage of iPAT in minimizing signal loss from regions that are prone to susceptibility artifacts. Although not demonstrated at a group level, the results from this study serves as a proof-of-concept that iPAT/SMS combination could be advantageous in resting state fcMRI studies, particularly at higher field strengths because of T2* shortening. Regions revealed (BAs 37 and 47) as positively correlated to the OFC seed is consistent with recent reports (Kahnt et al., 2012).

Chapter 5

General Conclusions

In this work we have demonstrated that the improved sensitivity of the 32Ch coil result in increased detection of functional connections and stronger correlation strengths, which potentially offer opportunity for smaller sample size in group level statistics, thereby preventing additional data collection. By the application of multichannel arrays in the clinical realm, we provide evidence for significant hyper-connectivity in the patient group as compared to controls in all the subcortical regions explored in the context of social anxiety disorder (SAD). In addition, we provide several novel findings, including alterations in regions that are known to be involved in emotional processing, but have not been reported in the realm of resting state fcMRI. Significantly enhanced seed-based functional connectivity of the globus pallidus with precuneus and the cerebellum with left amygdala in the patient group is particularly interesting as it brings basal ganglia and cerebellar regions to the forefront of understanding the neuronal mechanism of SAD. More studies are needed to validate these findings, which could provide better understanding of the pathophysiology of this disorder. Enhanced image SNR with the 32Ch coil from mid-brain regions as shown in this work could find potential applications in other neuropsychiatric disorders.

Finally, the optimization of acquisition protocol with slice-acceleration strategies such as simultaneous multi-slice (SMS) acquisition re-iterate the advantages of multichannel array coil (e.g., 32 elements or more) for higher temporal resolutions (TR=800 ms with SMS factors of 7). Proportionality of BOLD CNR with tSNR, and the improvements in tSNR with multichannel

arrays at high resolutions was taken into full consideration for the synergistic application of array coils and parallel imaging. The combination of higher temporal resolution and the 32Ch coil offer higher sensitivity in terms of revealing functional connections in the DMN, specifically at higher spatial resolutions, while maintaining whole-brain coverage. This is achieved at subsecond TR, whereas the TR had to be 6s to get the same coverage without the integration of SMS acquisition scheme, implying an improvement of almost an order of magnitude. Applications such as pharmacologic fMRI (for time-course analysis of the drug action) or hemodynamic response modeling (to investigate initial dip, or post-stimulus undershoot) could benefit directly from short TR.

It is plausible that the concerted effort of multichannel array coils and SMS acquisition can reduce TR and still maintain high-resolution acquisition without trading off tSNR. This translates to improvement in BOLD CNR and reductions in scan time as shown in this study. Since head motion (which tends to increase with increases in scantime) deteriorates tSNR, any effort to minimize scan time offers a positive impact to data quality. The tSNR of 32Ch coil, especially at higher temporal resolutions were remarkably better than that of the 12Ch coil, directly translating to significantly better fcMRI maps as shown in this work. Our characterization of multichannel arrays was performed on the particular design and coil manufacturer. Other multichannel arrays might offer different degree of sensitivity in the cortical brain areas compared to deeper structures due to variability in the design configuration/coil geometry. Finally, combining SMS acquisition and in-plane acceleration look promising for restoring functional connectivity from susceptibility prone regions. To attain higher spatial resolutions (<2mm iso) it might be beneficial to move towards higher magnetic field strengths (e.g., 7T) or higher N arrays such as 64Ch coil.

References

Achard S, Bullmore E. (2007): Efficiency and cost of economical brain functional networks. PLoS Comput Biol 3(2):e17.

Anteraper SA, Whitfield-Gabrieli S, Keil B, Shannon S, Gabrieli JD, Triantafyllou C. (2013): Exploring functional connectivity networks with multichannel brain array coils. Brain connectivity 3(3):302-15.

Arsalidou M, Duerden EG, Taylor MJ. (2012): The centre of the brain: Topographical model of motor, cognitive, affective, and somatosensory functions of the basal ganglia. Human brain mapping.

Ashburner J, Friston KJ. (2005): Unified segmentation. Neuroimage 26(3):839-51.

Baas D, Aleman A, Kahn RS. (2004): Lateralization of amygdala activation: a systematic review of functional neuroimaging studies. Brain research. Brain research reviews 45(2):96-103.

Ball TM, Sullivan S, Flagan T, Hitchcock CA, Simmons A, Paulus MP, Stein MB. (2012): Selective effects of social anxiety, anxiety sensitivity, and negative affectivity on the neural bases of emotional face processing. Neuroimage 59(2):1879-87.

Barry RL, Coaster M, Rogers BP, Newton AT, Moore J, Anderson AW, Zald DH, Gore JC. (2013): On the origins of signal variance in FMRI of the human midbrain at high field. Plos One 8(4):e62708.

Baumann O, Mattingley JB. (2012): Functional topography of primary emotion processing in the human cerebellum. Neuroimage 61(4):805-11.

Behzadi Y, Restom K, Liau J, Liu TT. (2007): A component based noise correction method (CompCor) for BOLD and perfusion based fMRI. NeuroImage 37(1):90-101.

Beraha E, Eggers J, Hindi Attar C, Gutwinski S, Schlagenhauf F, Stoy M, Sterzer P, Kienast T, Heinz A, Bermpohl F. (2012): Hemispheric asymmetry for affective stimulus processing in healthy subjects--a fMRI study. Plos One 7(10):e46931.

Biswal B, Yetkin FZ, Haughton VM, Hyde JS. (1995): Functional connectivity in the motor cortex of resting human brain using echo-planar MRI. Magnetic resonance in medicine : official journal of the Society of Magnetic Resonance in Medicine / Society of Magnetic Resonance in Medicine 34(4):537-41.

Buckner RL, Andrews-Hanna JR, Schacter DL. (2008): The brain's default network: anatomy, function, and relevance to disease. Ann N Y Acad Sci 1124:1-38.

Bullmore E, Sporns O. (2009): Complex brain networks: graph theoretical analysis of structural and functional systems. Nature reviews. Neuroscience 10(3):186-98.

Button KS, Ioannidis JP, Mokrysz C, Nosek BA, Flint J, Robinson ES, Munafo MR. (2013): Power failure: why small sample size undermines the reliability of neuroscience. Nat Rev Neurosci 14(5):365-76.

Cassimjee N, Fouche JP, Burnett M, Lochner C, Warwick J, Dupont P, Stein DJ, Cloete KJ, Carey PD. (2010): Changes in regional brain volumes in social anxiety disorder following 12 weeks of treatment with escitalopram. Metabolic brain disease 25(4):369-74.

Catenoix H, Magnin M, Guenot M, Isnard J, Mauguiere F, Ryvlin P. (2005): Hippocampal-orbitofrontal connectivity in human: an electrical stimulation study. Clinical neurophysiology : official journal of the International Federation of Clinical Neurophysiology 116(8):1779-84.

Chai XJ, Castanon AN, Ongur D, Whitfield-Gabrieli S. (2011): Anticorrelations in resting state networks without global signal regression. Neuroimage.

Chang C, Metzger CD, Glover GH, Duyn JH, Heinze HJ, Walter M. (2013): Association between heart rate variability and fluctuations in resting-state functional connectivity. Neuroimage 68:93-104.
Corbetta M, Shulman GL. (2002): Control of goal-directed and stimulus-driven attention in the brain. Nature reviews. Neuroscience 3(3):201-15.
Deichmann R, Josephs O, Hutton C, Corfield DR, Turner R. (2002): Compensation of susceptibility-induced BOLD sensitivity losses in echo-planar fMRI imaging. Neuroimage 15(1):120-35.
Di Martino A, Scheres A, Margulies DS, Kelly AM, Uddin LQ, Shehzad Z, Biswal B, Walters JR, Castellanos FX, Milham MP. (2008): Functional connectivity of human striatum: a resting state FMRI study. Cerebral cortex 18(12):2735-47.
Ding J, Chen H, Qiu C, Liao W, Warwick JM, Duan X, Zhang W, Gong Q. (2011): Disrupted functional connectivity in social anxiety disorder: a resting-state fMRI study. Magnetic resonance imaging 29(5):701-11.
Etkin A, Prater KE, Schatzberg AF, Menon V, Greicius MD. (2009): Disrupted amygdalar subregion functional connectivity and evidence of a compensatory network in generalized anxiety disorder. Archives of general psychiatry 66(12):1361-72.
Feinberg DA, Moeller S, Smith SM, Auerbach E, Ramanna S, Gunther M, Glasser MF, Miller KL, Ugurbil K, Yacoub E. (2010): Multiplexed echo planar imaging for sub-second whole brain FMRI and fast diffusion imaging. PloS one 5(12):e15710.
Feinberg DA, Setsompop K. (2013): Ultra-fast MRI of the human brain with simultaneous multi-slice imaging. Journal of magnetic resonance 229:90-100.
First MB, Spitzer RL, Gibbon M, Williams, JBW. (1995): Structured Clinical Interview for DSM-IV Axis I Disorder- Patient Edition (SCID-I/P). Biometrics Research Department, New York State Psychiatric Institute, New York.
Fox MD, Snyder AZ, Vincent JL, Corbetta M, Van Essen DC, Raichle ME. (2005): The human brain is intrinsically organized into dynamic, anticorrelated functional networks. Proceedings of the National Academy of Sciences of the United States of America 102(27):9673-8.
Fransson P. (2006): How default is the default mode of brain function? Further evidence from intrinsic BOLD signal fluctuations. Neuropsychologia 44(14):2836-45.
Freitas-Ferrari MC, Hallak JE, Trzesniak C, Filho AS, Machado-de-Sousa JP, Chagas MH, Nardi AE, Crippa JA. (2010): Neuroimaging in social anxiety disorder: a systematic review of the literature. Progress in neuro-psychopharmacology & biological psychiatry 34(4):565-80.
Frick A, Howner K, Fischer H, Eskildsen SF, Kristiansson M, Furmark T. (2013): Cortical thickness alterations in social anxiety disorder. Neuroscience letters 536:52-5.
Friston K. 2007. Statistical parametric mapping: the analysis of functional brain images. Amsterdam; Boston: Elsevier/Academic Press.
Gentili C, Ricciardi E, Gobbini MI, Santarelli MF, Haxby JV, Pietrini P, Guazzelli M. (2009): Beyond amygdala: Default Mode Network activity differs between patients with social phobia and healthy controls. Brain research bulletin 79(6):409-13.
Gimenez M, Pujol J, Ortiz H, Soriano-Mas C, Lopez-Sola M, Farre M, Deus J, Merlo-Pich E, Martin-Santos R. (2012): Altered brain functional connectivity in relation to perception of scrutiny in social anxiety disorder. Psychiatry Research 202(3):214-23.

Goldin P, Ziv M, Jazaieri H, Gross JJ. (2012): Randomized controlled trial of mindfulness-based stress reduction versus aerobic exercise: effects on the self-referential brain network in social anxiety disorder. Frontiers in human neuroscience 6:295.
Gorno-Tempini ML, Hutton C, Josephs O, Deichmann R, Price C, Turner R. (2002): Echo time dependence of BOLD contrast and susceptibility artifacts. Neuroimage 15(1):136-42.
Greicius MD, Krasnow B, Reiss AL, Menon V. (2003): Functional connectivity in the resting brain: a network analysis of the default mode hypothesis. Proc Natl Acad Sci U S A 100(1):253-8.
Griswold MA, Jakob PM, Heidemann RM, Nittka M, Jellus V, Wang J, Kiefer B, Haase A. (2002): Generalized autocalibrating partially parallel acquisitions (GRAPPA). Magnetic resonance in medicine : official journal of the Society of Magnetic Resonance in Medicine / Society of Magnetic Resonance in Medicine 47(6):1202-10.
Hahn A, Stein P, Windischberger C, Weissenbacher A, Spindelegger C, Moser E, Kasper S, Lanzenberger R. (2011): Reduced resting-state functional connectivity between amygdala and orbitofrontal cortex in social anxiety disorder. Neuroimage 56(3):881-889.
Hasler G, Fromm S, Alvarez RP, Luckenbaugh DA, Drevets WC, Grillon C. (2007): Cerebral blood flow in immediate and sustained anxiety. The Journal of neuroscience : the official journal of the Society for Neuroscience 27(23):6313-9.
Hattingh CJ, Ipser J, Tromp SA, Syal S, Lochner C, Brooks SJ, Stein DJ. (2012): Functional magnetic resonance imaging during emotion recognition in social anxiety disorder: an activation likelihood meta-analysis. Frontiers in human neuroscience 6:347.
Hayes CE, Axel L. (1985): Noise performance of surface coils for magnetic resonance imaging at 1.5 T. Medical physics 12(5):604-7.
Honey CJ, Kotter R, Breakspear M, Sporns O. (2007): Network structure of cerebral cortex shapes functional connectivity on multiple time scales. Proceedings of the National Academy of Sciences of the United States of America 104(24):10240-5.
Hutton C, Josephs O, Stadler J, Featherstone E, Reid A, Speck O, Bernarding J, Weiskopf N. (2011): The impact of physiological noise correction on fMRI at 7T. NeuroImage 57(1):101-12.
Jones DT, Mateen FJ, Lucchinetti CF, Jack CR, Jr., Welker KM. (2011): Default mode network disruption secondary to a lesion in the anterior thalamus. Archives of neurology 68(2):242-7.
Kahnt T, Chang LJ, Park SQ, Heinzle J, Haynes JD. (2012): Connectivity-based parcellation of the human orbitofrontal cortex. J Neurosci 32(18):6240-50.
Keil B, Alagappan V, Mareyam A, McNab JA, Fujimoto K, Tountcheva V, Triantafyllou C, Dilks DD, Kanwisher N, Lin W and others. (2011): Size-optimized 32-channel brain arrays for 3 T pediatric imaging. Magnetic resonance in medicine : official journal of the Society of Magnetic Resonance in Medicine / Society of Magnetic Resonance in Medicine 66(6):1777-87.
Keil B, Blau JN, Biber S, Hoecht P, Tountcheva V, Setsompop K, Triantafyllou C, Wald LL. (2012): A 64-channel 3T array coil for accelerated brain MRI. Magnetic resonance in medicine : official journal of the Society of Magnetic Resonance in Medicine / Society of Magnetic Resonance in Medicine.
Kellman P, McVeigh ER. (2005): Image reconstruction in SNR units: a general method for SNR measurement. Magnetic resonance in medicine : official journal of the Society of

Magnetic Resonance in Medicine / Society of Magnetic Resonance in Medicine 54(6):1439-47.
Kelly AM, Di Martino A, Uddin LQ, Shehzad Z, Gee DG, Reiss PT, Margulies DS, Castellanos FX, Milham MP. (2009): Development of anterior cingulate functional connectivity from late childhood to early adulthood. Cerebral cortex 19(3):640-57.
Kessler RC, Chiu WT, Demler O, Merikangas KR, Walters EE. (2005): Prevalence, severity, and comorbidity of 12-month DSM-IV disorders in the National Comorbidity Survey Replication. Archives of general psychiatry 62(6):617-27.
Klumpers UM, Veltman DJ, Drent ML, Boellaard R, Comans EF, Meynen G, Lammertsma AA, Hoogendijk WJ. (2010): Reduced parahippocampal and lateral temporal GABAA-[11C]flumazenil binding in major depression: preliminary results. European journal of nuclear medicine and molecular imaging 37(3):565-74.
Knake S, Triantafyllou C, Wald LL, Wiggins G, Kirk GP, Larsson PG, Stufflebeam SM, Foley MT, Shiraishi H, Dale AM and others. (2005): 3T phased array MRI improves the presurgical evaluation in focal epilepsies: a prospective study. Neurology 65(7):1026-31.
Lancaster JL, Woldorff MG, Parsons LM, Liotti M, Freitas CS, Rainey L, Kochunov PV, Nickerson D, Mikiten SA, Fox PT. (2000): Automated Talairach atlas labels for functional brain mapping. Human brain mapping 10(3):120-31.
Lauterbach EC, Spears TE, Prewett MJ, Price ST, Jackson JG, Kirsh AD. (1994): Neuropsychiatric disorders, myoclonus, and dystonia in calcification of basal ganglia pathways. Biological psychiatry 35(5):345-51.
Lenglet C, Abosch A, Yacoub E, De Martino F, Sapiro G, Harel N. (2012): Comprehensive in vivo mapping of the human basal ganglia and thalamic connectome in individuals using 7T MRI. Plos One 7(1):e29153.
Liao W, Chen H, Feng Y, Mantini D, Gentili C, Pan Z, Ding J, Duan X, Qiu C, Lui S and others. (2010a): Selective aberrant functional connectivity of resting state networks in social anxiety disorder. Neuroimage 52(4):1549-58.
Liao W, Qiu CJ, Gentili C, Walter M, Pan ZY, Ding JR, Zhang W, Gong QY, Chen HF. (2010b): Altered Effective Connectivity Network of the Amygdala in Social Anxiety Disorder: A Resting-State fMRI Study. Plos One 5(12).
Liao W, Xu Q, Mantini D, Ding JR, Machado-de-Sousa JP, Hallak JEC, Trzesniak C, Qiu CJ, Zeng L, Zhang W and others. (2011): Altered gray matter morphometry and resting-state functional and structural connectivity in social anxiety disorder. Brain Research 1388:167-177.
Liebowitz MR. (1987): Social Phobia. Modern Problems of Pharmacopsychiatry, 22: 141-173.
Ligot N, Krystkowiak P, Simonin C, Goldman S, Peigneux P, Van Naemen J, Monclus M, Lacroix SF, Devos D, Dujardin K and others. (2011): External globus pallidus stimulation modulates brain connectivity in Huntington's disease. Journal of cerebral blood flow and metabolism : official journal of the International Society of Cerebral Blood Flow and Metabolism 31(1):41-6.
Lipsman N, Woodside DB, Giacobbe P, Hamani C, Carter JC, Norwood SJ, Sutandar K, Staab R, Elias G, Lyman CH and others. (2013): Subcallosal cingulate deep brain stimulation for treatment-refractory anorexia nervosa: a phase 1 pilot trial. Lancet 381(9875):1361-70.

Lorberbaum JP, Kose S, Johnson MR, Arana GW, Sullivan LK, Hamner MB, Ballenger JC, Lydiard RB, Brodrick PS, Bohning DE and others. (2004): Neural correlates of speech anticipatory anxiety in generalized social phobia. Neuroreport 15(18):2701-5.
Maldjian JA, Laurienti PJ, Burdette JH. (2004): Precentral gyrus discrepancy in electronic versions of the Talairach atlas. NeuroImage 21(1):450-5.
Maldjian JA, Laurienti PJ, Kraft RA, Burdette JH. (2003): An automated method for neuroanatomic and cytoarchitectonic atlas-based interrogation of fMRI data sets. NeuroImage 19(3):1233-9.
Marchand WR, Lee JN, Thatcher JW, Thatcher GW, Jensen C, Starr J. (2007): Motor deactivation in the human cortex and basal ganglia. Neuroimage 38(3):538-48.
Marchand WR. (2010): Cortico-basal ganglia circuitry: a review of key research and implications for functional connectivity studies of mood and anxiety disorders. Brain structure & function 215(2):73-96.
Medina JF, Repa JC, Mauk MD, LeDoux JE. (2002): Parallels between cerebellum- and amygdala-dependent conditioning. Nature reviews. Neuroscience 3(2):122-31.
Mumford JA, Nichols TE. (2008): Power calculation for group fMRI studies accounting for arbitrary design and temporal autocorrelation. NeuroImage 39(1):261-8.
Pannekoek JN, Veer IM, van Tol MJ, van der Werff SJ, Demenescu LR, Aleman A, Veltman DJ, Zitman FG, Rombouts SA, van der Wee NJ. (2012): Resting-state functional connectivity abnormalities in limbic and salience networks in social anxiety disorder without comorbidity. European neuropsychopharmacology : the journal of the European College of Neuropsychopharmacology.
Perez-Edgar K, Hardee JE, Guyer AE, Benson BE, Nelson EE, Gorodetsky E, Goldman D, Fox NA, Pine DS, Ernst M. (2013): DRD4 and striatal modulation of the link between childhood behavioral inhibition and adolescent anxiety. Social cognitive and affective neuroscience.
Power JD, Barnes KA, Snyder AZ, Schlaggar BL, Petersen SE. (2012): Spurious but systematic correlations in functional connectivity MRI networks arise from subject motion. Neuroimage 59(3):2142-54.
Prater KE, Hosanagar A, Klumpp H, Angstadt M, Luan Phan K. (2013): Aberrant amygdala-frontal cortex connectivity during perception of fearful faces and at rest in generalized social anxiety disorder. Depression and anxiety 30(3):234-41.
Qiu C, Liao W, Ding J, Feng Y, Zhu C, Nie X, Zhang W, Chen H, Gong Q. (2011): Regional homogeneity changes in social anxiety disorder: a resting-state fMRI study. Psychiatry Research 194(1):47-53.
Qiu MG, Ye Z, Li QY, Liu GJ, Xie B, Wang J. (2010): Changes of Brain Structure and Function in ADHD Children. Brain topography.
Raichle ME, MacLeod AM, Snyder AZ, Powers WJ, Gusnard DA, Shulman GL. (2001): A default mode of brain function. Proc Natl Acad Sci U S A 98(2):676-82.
Roemer PB, Edelstein WA, Hayes CE, Souza SP, Mueller OM. (1990): The NMR phased array. Magnetic resonance in medicine : official journal of the Society of Magnetic Resonance in Medicine / Society of Magnetic Resonance in Medicine 16(2):192-225.
Rubinov M, Sporns O. (2010): Complex network measures of brain connectivity: uses and interpretations. Neuroimage 52(3):1059-69.

Sang L, Qin W, Liu Y, Han W, Zhang Y, Jiang T, Yu C. (2012): Resting-state functional connectivity of the vermal and hemispheric subregions of the cerebellum with both the cerebral cortical networks and subcortical structures. Neuroimage 61(4):1213-25.
Satterthwaite TD, Wolf DH, Loughead J, Ruparel K, Elliott MA, Hakonarson H, Gur RC, Gur RE. (2012): Impact of in-scanner head motion on multiple measures of functional connectivity: relevance for studies of neurodevelopment in youth. Neuroimage 60(1):623-32.
Seeley WW, Menon V, Schatzberg AF, Keller J, Glover GH, Kenna H, Reiss AL, Greicius MD. (2007): Dissociable intrinsic connectivity networks for salience processing and executive control. The Journal of neuroscience : the official journal of the Society for Neuroscience 27(9):2349-56.
Setsompop K, Gagoski BA, Polimeni JR, Witzel T, Wedeen VJ, Wald LL. (2012): Blipped-controlled aliasing in parallel imaging for simultaneous multislice echo planar imaging with reduced g-factor penalty. Magn Reson Med 67(5):1210-24.
Sheline YI, Barch DM, Donnelly JM, Ollinger JM, Snyder AZ, Mintun MA. (2001): Increased amygdala response to masked emotional faces in depressed subjects resolves with antidepressant treatment: an fMRI study. Biological psychiatry 50(9):651-8.
Sheline YI, Price JL, Yan Z, Mintun MA. (2010): Resting-state functional MRI in depression unmasks increased connectivity between networks via the dorsal nexus. Proceedings of the National Academy of Sciences of the United States of America 107(24):11020-5.
Sladky R, Baldinger P, Kranz GS, Trostl J, Hoflich A, Lanzenberger R, Moser E, Windischberger C. (2013): High-resolution functional MRI of the human amygdala at 7 T. European journal of radiology 82(5):728-33.
Sridharan D, Levitin DJ, Menon V. (2008): A critical role for the right fronto-insular cortex in switching between central-executive and default-mode networks. Proceedings of the National Academy of Sciences of the United States of America 105(34):12569-74.
Sutherland MT, McHugh MJ, Pariyadath V, Stein EA. (2012): Resting state functional connectivity in addiction: Lessons learned and a road ahead. NeuroImage.
Talati A, Pantazatos SP, Schneier FR, Weissman MM, Hirsch J. (2013): Gray matter abnormalities in social anxiety disorder: primary, replication, and specificity studies. Biological psychiatry 73(1):75-84.
Taylor KS, Seminowicz DA, Davis KD. (2009): Two systems of resting state connectivity between the insula and cingulate cortex. Human brain mapping 30(9):2731-45.
Thayer JF, Ahs F, Fredrikson M, Sollers JJ, 3rd, Wager TD. (2012): A meta-analysis of heart rate variability and neuroimaging studies: implications for heart rate variability as a marker of stress and health. Neuroscience and biobehavioral reviews 36(2):747-56.
Tomasi D, Volkow ND. (2011): Functional connectivity hubs in the human brain. NeuroImage 57(3):908-17.
Triantafyllou C, Hoge RD, Krueger G, Wiggins CJ, Potthast A, Wiggins GC, Wald LL. (2005): Comparison of physiological noise at 1.5 T, 3 T and 7 T and optimization of fMRI acquisition parameters. Neuroimage 26(1):243-50.
Triantafyllou C, Polimeni JR, Wald LL. (2011): Physiological noise and signal-to-noise ratio in fMRI with multichannel array coils. NeuroImage 55(2):597-606.
van der Kouwe AJ, Benner T, Fischl B, Schmitt F, Salat DH, Harder M, Sorensen AG, Dale AM. (2005): On-line automatic slice positioning for brain MR imaging. NeuroImage 27(1):222-30.

van der Wee NJ, van Veen JF, Stevens H, van Vliet IM, van Rijk PP, Westenberg HG. (2008): Increased serotonin and dopamine transporter binding in psychotropic medication-naive patients with generalized social anxiety disorder shown by 123I-beta-(4-iodophenyl)-tropane SPECT. Journal of nuclear medicine : official publication, Society of Nuclear Medicine 49(5):757-63.

Van Dijk KR, Hedden T, Venkataraman A, Evans KC, Lazar SW, Buckner RL. (2010): Intrinsic functional connectivity as a tool for human connectomics: theory, properties, and optimization. Journal of neurophysiology 103(1):297-321.

Van Dijk KR, Sabuncu MR, Buckner RL. (2012): The influence of head motion on intrinsic functional connectivity MRI. Neuroimage 59(1):431-8.

Veit R, Flor H, Erb M, Hermann C, Lotze M, Grodd W, Birbaumer N. (2002): Brain circuits involved in emotional learning in antisocial behavior and social phobia in humans. Neuroscience letters 328(3):233-6.

Vincent JL, Kahn I, Snyder AZ, Raichle ME, Buckner RL. (2008): Evidence for a frontoparietal control system revealed by intrinsic functional connectivity. Journal of neurophysiology 100(6):3328-42.

Ward AM, Schultz AP, Huijbers W, Van Dijk KR, Hedden T, Sperling RA. (2013): The parahippocampal gyrus links the default-mode cortical network with the medial temporal lobe memory system. Human brain mapping.

Warwick JM, Carey PD, Cassimjee N, Lochner C, Hemmings S, Moolman-Smook H, Beetge E, Dupont P, Stein DJ. (2012): Dopamine transporter binding in social anxiety disorder: the effect of treatment with escitalopram. Metabolic brain disease 27(2):151-8.

Whitfield-Gabrieli S, Nieto Castanon A. (2012): Conn: A functional connectivity toolbox for correlated and anticorrelated brain networks. Brain connectivity.

Wiesinger F, Boesiger P, Pruessmann KP. (2004): Electrodynamics and ultimate SNR in parallel MR imaging. Magnetic resonance in medicine : official journal of the Society of Magnetic Resonance in Medicine / Society of Magnetic Resonance in Medicine 52(2):376-90.

Wiggins GC, Polimeni JR, Potthast A, Schmitt M, Alagappan V, Wald LL. (2009): 96-Channel receive-only head coil for 3 Tesla: design optimization and evaluation. Magnetic resonance in medicine : official journal of the Society of Magnetic Resonance in Medicine / Society of Magnetic Resonance in Medicine 62(3):754-62.

Wiggins GC, Triantafyllou C, Potthast A, Reykowski A, Nittka M, Wald LL. (2006): 32-channel 3 Tesla receive-only phased-array head coil with soccer-ball element geometry. Magnetic resonance in medicine : official journal of the Society of Magnetic Resonance in Medicine / Society of Magnetic Resonance in Medicine 56(1):216-23.

Zhang D, Raichle ME. (2010): Disease and the brain's dark energy. Nature reviews. Neurology 6(1):15-28.